Experimental study of exhaust temperature variation in a homogeneous charge compression ignition engine

M Shahbakhti[1], **A Ghazimirsaied**[2], and **C R Koch**[2*]
[1]Department of Mechanical Engineering, KNT University of Technology, Tehran, Iran
[2]Department of Mechanical Engineering, University of Alberta, Edmonton, Canada

The manuscript was received on 28 December 2009 and was accepted after revision for publication on 30 April 2010.

DOI: 10.1243/09544070JAUTO1473

Abstract: Homogeneous charge compression ignition (HCCI) engines have low nitrogen oxide and particulate matter engine-out emissions but have higher unburned hydrocarbon and carbon monoxide emissions than the conventional spark ignition (SI) and diesel engines do. Only for sufficiently high exhaust gas temperatures can an exhaust after-treatment be used; thus a low exhaust gas temperature in certain operating conditions can limit the operating range in HCCI engines. The influences of the engine conditions on the exhaust gas temperature in a single-cylinder experimental engine are investigated at 340 steady state operating points. The variation in the exhaust gas temperature is also studied under transient conditions and during mode switching between SI and HCCI combustion. For the conditions tested, a significant number of data have an exhaust gas temperature below 300 °C which is below the light-off temperature of typical catalytic converters on the market. Three different categories of engine variables are recognized and classified by how the exhaust temperature is affected by changing that variable. The first category is defined as the primary variables (e.g. the intake pressure and the fuel octane number) for which the location of ignition timing is the dominant factor in influencing the exhaust temperature. The other groups include compounding variables such as the engine speed and opposing variables such as the intake temperature, the coolant temperature, and the equivalence ratio. In addition, experimental results show that the exhaust temperature for HCCI engines is not strongly dependent on the engine load, unlike that for SI engines where the engine load is a main factor in determining the exhaust temperature.

Keywords: homogeneous charge compression ignition, exhaust temperature, emissions, primary reference fuel

1 INTRODUCTION

Homogeneous charge compression ignition (HCCI) is a combustion mode that can provide diesel-like engine efficiency and generates ultra-low engine-out nitrogen oxide (NO_x) and particulate matter emissions [**1**, **2**]. The principle of this combustion mode is based on the autoignition of a highly diluted or lean air-to-fuel ratio (AFR) mixture which allows an HCCI engine to run with a fuel consumption advantage over conventional spark ignition (SI) and diesel engines. Low-temperature combustion caused by the presence of excess air and dilutents suppresses the rate of NO_x formation. Burning of the premixed lean mixture and the absence of diffusion-limited combustion virtually remove the potential for soot formation in HCCI engines [**3**]. These factors may eliminate the requirement for NO_x and soot after-treatment systems [**1**].

Despite ultra-low NO_x and negligible soot emissions from HCCI engines, hydrocarbon (HC) and carbon monoxide (CO) emissions are normally higher than those from diesel engines [**3**]. However, reducing HC and CO emissions from HCCI engines

**Corresponding author: Department of Mechanical Engineering, University of Alberta, Edmonton, Alberta, T6G 2G8, Canada.*
email: bob.koch@ualberta.ca

is easier than reducing NO_x and soot emissions from diesel engines [**4**]. High HC and CO emissions from HCCI engines are mainly due to the low in-cylinder temperature caused by lean-burn or high-dilution combustion. This can result in incomplete combustion and a decrease in post-combustion oxidation rates inside the cylinder [**1**, **3**]. Results show that the CO-to-carbon dioxide (CO_2) reactions in HCCI are sensitive to the combustion temperature, and a minimum peak temperature of 1500 K is required to oxidize CO [**5**]. As the charge is made leaner by decreasing fuelling, the production of HCs and CO is dominated by incomplete bulk-gas reactions [**6**, **7**]. Higher HC and CO emissions were also observed in the work reported in reference [**8**] when the equivalence ratio was decreased for an HCCI engine fuelled with blends of iso-octane and *n*-heptane.

High HC and CO engine-out emissions from HCCI engines can be mitigated by using oxidation catalysts which can reach conversion efficiencies of up to 95 per cent for HC and CO pollutants when the catalytic converter is fully warmed [**9**]. The catalytic converter must reach its operating temperature to be effective. The light-off temperature (the temperature at which the catalyst becomes more than 50 per cent effective) is about 250–300 °C for most catalysts [**10**–**13**]. The light-off temperature depends on the active catalytic material and thermal inertia of the catalyst and it can be as high as 400 °C [**14**]. The light-off temperature can be reduced to 200 °C by using an advanced new catalyst formulation [**15**] or by using a modified catalyst material with a higher cell density and thinner-wall substrates [**14**]. However, this significantly increases the cost of catalytic converters. Methods to reduce the light-off time in catalysts are generally classified into active or passive systems. Typical active systems include electrically heated catalysts [**16**], fuel burners [**17**], secondary air injection [**18**], and after-burners [**19**], all of which require an extra energy supply. In contrast, passive systems rely mainly on thermal management of the energy obtained from exhaust gases (e.g. by using a close-coupled catalyst [**20**] or by using low-thermal-inertia manifolds [**12**]). The disadvantages of active systems are a higher fuel consumption rate, more complexity, and higher initial cost [**21**]. Passive systems, however, are completely dependent on the temperature and flowrate of the exhaust gases. Since HCCI typically has a low exhaust temperature, as low as 120 °C [**22**], the HC and CO abatement by oxidation catalysts remains an important concern in HCCI engines. This could limit the desirable operating range of HCCI engines and also the low HCCI exhaust temperature provides little energy for turbocharging, which is often used to extend the HCCI operating range for high loads [**23**]. Understanding the factors influencing the HCCI exhaust temperature is essential for better modulation of the engine charge variables to extend the HCCI operating range while maintaining exhaust temperatures high enough for the catalyst.

This paper is, to the present authors' knowledge, the first detailed analysis of the variations in the exhaust temperature in HCCI engines. However, aspects of the HCCI exhaust temperature have been investigated. In reference [**24**], cycle-to-cycle variations in the exhaust temperature and its relation to combustion phasing were discussed for a camless gasoline HCCI engine which operates with an early exhaust-valve-closing strategy. It was found that the exhaust temperature at the end of the expansion stroke does not affect the HCCI combustion phasing for the next cycle; instead, combustion phasing is influenced by the gas temperature at the beginning of the compression stroke. The results in reference [**25**] indicated an increase in the exhaust gas temperature when the equivalence ratio is increased for a medium-duty direct-injection (DI) HCCI engine.

This study uses experimental data at over 340 steady state and transient operating conditions to investigate the sensitivity of the exhaust temperature to several charge variables in a range of engine loads. The primary aim of this study is to provide detailed results and discussion of the variables affecting the exhaust temperature in an HCCI engine. These results can be used to understand HCCI combustion further so that effective control strategies, based on physical arguments, can be developed in the future. In addition, since a dual-mode HCCI–SI combustion is useful for extending the HCCI operating range [**26**], the variation in the exhaust temperature during mode switching and the difference between these two modes are described.

In this paper, first the experimental set-up is explained and then the HCCI experimental conditions are described. Next, the experimental results are presented and discussed; finally, a summary of the results are provided and conclusions are reached.

2 EXPERIMENTAL ENGINE SET-UP

In this work, experimental measurements based on a single-cylinder Ricardo Mark III engine with Rover K7 head are recorded. The Ricardo engine has a

combustion chamber with pent-roof design with a centrally located spark plug and it uses a flat-top cast aluminium piston with valve reliefs. Dual camshafts located in the cylinder head operate two intake and two exhaust valves. Table 1 indicates the timing of the valves as well as the engine geometry.

A schematic diagram of the experimental set-up is shown in Fig. 1. Two separate fuel systems with a fuel pressure of 3 bar are used, and the injection timing is set to ensure injection when the intake valves close. One of the fuel systems is used to inject *n*-heptane and the other is used to inject iso-octane. The separate flowrate control of each of these two fuels allows any desired octane number (ON) to be obtained. Both the *n*-heptane and the iso-octane injectors are aimed directly at the back of the intake valves. First, the fresh intake air entering the engine is passed through a laminar airflow meter for flowrate measurement. Then, the fresh charge is mixed with recirculated hot exhaust gases using an insulated return line from the exhaust to the intake manifold. Next, a supercharger driven by a variable-speed electric motor adjusts the intake manifold pressure and then a 600 W electrical band-type heater sets the mixture temperature to the desired value using a closed-loop controller. Finally, the exhaust gases exiting the cylinder are sampled for emission analysis. As shown in Fig. 1, the emission can be sampled either from the intake manifold or from the exhaust manifold.

Table 1 Configurations of the Ricardo single-cylinder engine (ABDC, after bottom dead centre)

Parameter (units)	Value
Bore (mm)	80
Stroke (mm)	88.9
Compression ratio	10
Displacement (l)	0.447
Number of valves	4
Intake valve opening (deg CA ABDC)	−175
Intake valve closing* (deg CA ABDC)	55
Exhaust valve opening (deg CA ABDC)	−70
Exhaust valve closing (deg CA ABDC)	−175

*The valve closing point is defined at a valve lift of 0.15 mm [**10**].

The engine-out AFR value is measured with an ECM AFRecorder 1200 universal exhaust gas oxygen sensor which has a measurement accuracy of 0.01–0.03. The intake temperature is measured with 2 °C resolution using a K-type thermocouple positioned in the intake manifold before the charge entering the cylinder. A $\frac{1}{32}$ in sheathed J-type thermocouple is used for fast exhaust temperature measurement. The thermocouple is placed in the exhaust as closely as possible to the exhaust valve. The thermocouple voltage is amplified before sending to the data-logging system and is sampled every degree crank angle (CA). A polynomial fit outlined in reference [**27**] is used to calculate the temperature from the amplified voltage signal. The exhaust gas recirculation rate is determined by comparing the CO_2 concentrations in the intake and exhaust manifolds, and by assuming that all CO_2 in the intake manifold is from the exhaust gases. Measurement of the

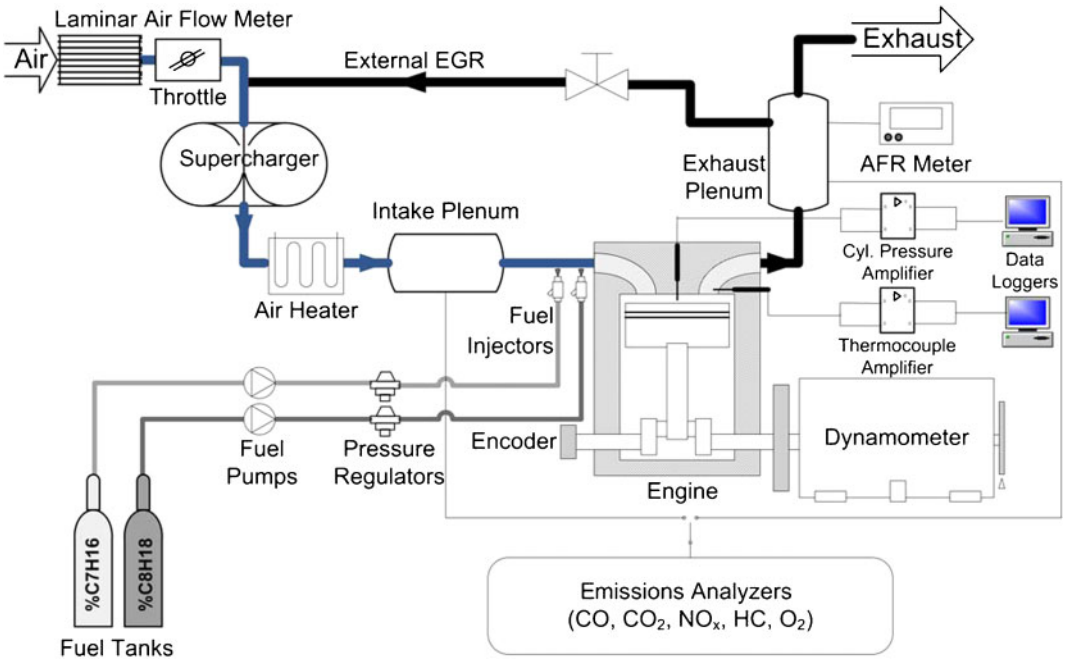

Fig. 1 Ricardo single-cylinder testbench schematic diagram (EGR, exhaust gas recirculation)

cylinder pressure is made using a Kistler water-cooled ThermoCOMP (model 6043A60) piezoelectric pressure sensor that is flush mounted in the cylinder head. CA measurement with 0.1° resolution is made using a BEI optical encoder connected to the crankshaft on the front of the engine. A five-gas emissions test bench is used to collect emissions data. NO_x is measured with 1 ppm resolution using a Horriba CLA-510SS emission analyser, HC is measured with 10 ppm resolution using a Horiba FIZ-510 emission analyser, and CO is measured with 0.01 per cent resolution using a Siemens ULTRAMAT 6 emission analyser.

The Ricardo engine is run to collect two types of experimental measurement: steady state points and transient points. Table 2 details the experimental conditions of the 340 steady state points used in this study. Steady state points include operation of the engine in both the HCCI and the SI modes. The indicated mean effective pressure (IMEP) of the engine ranges between 3.8 bar and 9.2 bar in the HCCI mode and between 5.2 bar and 11.8 bar in the SI mode. The low compression ratio of the Ricardo engine results in HCCI operation only for lower-ON fuels and at lower engine speeds. The primary reference fuel (PRF) number of 40 (denoted PRF 40) for the Ricardo engine is the highest for which HCCI operation is possible for a range of loads. All SI test points are run with pure iso-octane (PRF 100) in stoichiometric operation and the spark timing is adjusted to give a CA where 50 per cent of the fuel mass fraction is burned (denoted CA_{50}) of about 8 CA after top dead centre (ATDC) [**28**].

For each steady state test point, pressure traces from 200 consecutive engine cycles with 0.1° CA resolution are recorded. The start of combustion in HCCI is determined using the third derivative of the pressure trace criteria [**29**, **30**]. The Rassweiler–Withrow [**31**] method is used to calculate CA_{50} and the net heat release rate is determined using the usual heat release method [**10**] which applies the first law analysis to the engine charge assuming ideal-gas properties. Burn duration (BD) is defined as the difference between the CAs of 10 per cent and 90 per cent heat released. A pressure rise rate of 7 bar/deg CA is defined as the threshold for the knock limit [**28**] and a heuristically chosen limit of 5 per cent of the coefficient of variation in the indicated mean effective pressure is found to be the limit of misfire for the Ricardo engine [**32**]. Details about the cyclic variations in the IMEP and ignition timing for the Ricardo engine have been documented in reference [**29**].

Transient tests include interzonal (HCCI–HCCI) and mode-switching (SI–HCCI) experiments. HCCI–HCCI transient experiments are performed by transient fuelling at a constant air flowrate. The fuel injection pulse width is open loop scheduled by a dSpace MicroAutobox 1401/1501 engine control unit (ECU) to achieve the desired Φ and ON. The injected fuel mass per cycle for both injectors is estimated from the pulse width of the injectors [**33**]. The SI–HCCI transitions are enabled by programming the ECU with an open-loop look-up table for fuelling, in both the SI and the HCCI modes. A software switch is used to command the engine from the stoichiometric SI mode to the HCCI mode [**28**]. During each transient test, 450 cycles of cylinder pressure data are recorded with 0.1° CA resolution, and other engine variables are measured at a constant sample rate of 100 Hz.

Table 2 Operating conditions for the 340 steady state data points used in this study

	Value for the following engines	
Variable (units)	HCCI	SI
Number of points	304	36
Fuel (PRF*)	0–40	100
Engine speed N (r/min)	800–1340	1000–2000
Intake manifold temperature T_m (°C)	59–162	30–49
Equivalence ratio Φ	0.29–0.83	1.0
Intake manifold pressure P_m (kPa)	88–161	60–111
EGR (%)	0–30	0
Spark timing (deg CA ATDC)	—	$CA_{50} \approx 8$
Coolant temperature $T_{coolant}$ (°C)	41–84	80–86
Exhaust temperature T_{exh} (°C)	242–418	517–675

*The PRF number is defined as the volume percentage of iso-octane in the fuel mixture of *n*-heptane (PRF 0) and iso-octane (PRF 100).

3 RESULTS AND DISCUSSION

In this section the exhaust gas temperature T_{exh} is experimentally documented and the effects of the engine variables are investigated. First, the range of experimental T_{exh} highlights the significance of T_{exh} with respect to HCCI emissions. Next, the influences of several engine variables on T_{exh} are studied. Finally, the differences between the variation in T_{exh} in the HCCI mode and in the SI mode are discussed.

HCCI emissions and the IMEP of the Ricardo engine versus T_{exh} are shown in Fig. 2. The results in Fig. 2 show that T_{exh} can be as low as 242 °C in the HCCI mode and a significant portion of the data points have T_{exh} lower than typical catalyst light-off temperatures, 92 of the HCCI data points having T_{exh} lower than or equal to 300 °C. All the data points with low exhaust temperature ($T_{exh} \leqslant 300$ °C) have negli-

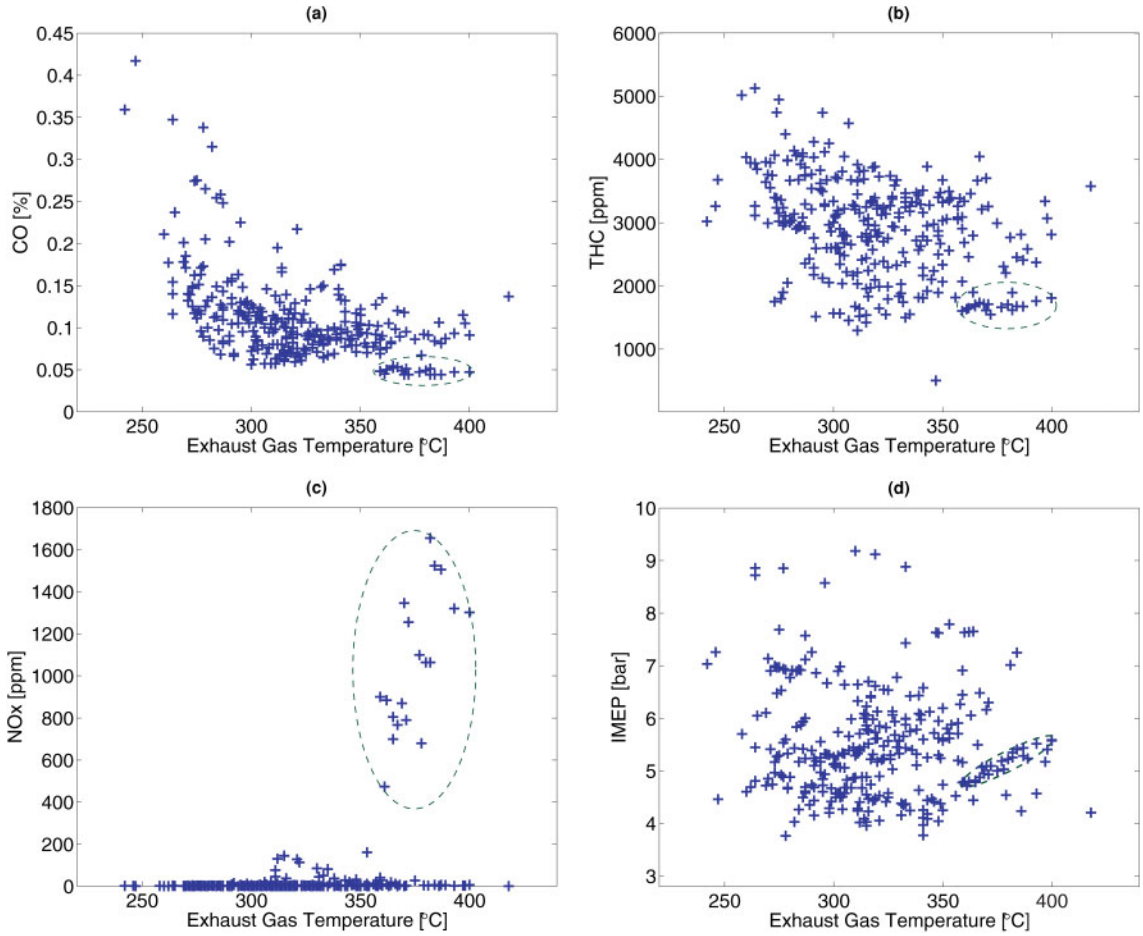

Fig. 2 Trend of variation in the HCCI exhaust gas emissions and IMEP with the exhaust gas temperature in an HCCI steady state operation

gible NO_x emissions and have a reasonable IMEP. These are desirable HCCI operating points, but the low T_{exh} at these points is a limiting factor for oxidizing HC and CO pollutants in the catalytic converters. The range of T_{exh} in Fig. 2 depends on the operating conditions in which the HCCI engine can run without exceeding the knock or misfiring limit. The HCCI exhaust temperature can be as low as 120 °C [**22**]. The peak T_{exh} among 304 HCCI data points in Fig. 2 is about 400 °C. This peak temperature is considered low compared with that of the SI mode for which the exhaust temperature is generally higher than 400 °C [**22**].

Higher HC and CO emissions are observed at lower T_{exh} in Figs 2(a) and (b). This makes the HCCI problem worse, since T_{exh} is low in these conditions; thus, a lower oxidation rate by a catalytic converter is expected despite having higher HC and CO emissions. Having higher HC and CO emissions at lower T_{exh} may be explained by having a lower in-cylinder gas temperature during the expansion stroke which reduces the possibility that post-oxidation reactions occur. High-NO_x-emission points in the dashed ellipse in Fig. 2(c) means undesirable HCCI operation (see data points 164 to 182 in Appendix 2). These data points are fuel rich ($0.6 \leqslant \Phi \leqslant 0.72$) and exhibit knocking characteristics with a pressure rise rate of 7.4–11.4 bar/deg CA and a knock intensity of 0.4–2.2 bar based on the PPmax metric. (PPmax is the maximum peak-to-peak value of the bandpass-filtered pressure trace and is a representative knock indicator which measures the intensity of knock-induced vibrations [**34**].) These high-NO_x data points are delineated by the dashed ellipses in Figs 2(a) and (b) and they are among the points with the lowest CO and HC emissions. The high combustion temperature for these fuel-rich data points results in high NO_x emission but low CO and HC emissions. These data points also have the highest T_{exh} values in the T_{exh} range indicated in Fig. 2.

3.1 Influences of the operating variables on T_{exh}

The engine charge variables predominantly determine the onset of autoignition and combustion

characteristics of HCCI engines. To investigate this systematically, each engine input is changed while maintaining the others constant. The six engine inputs that are varied are: intake pressure P_m; octane number ON; engine speed N; intake temperature T_m; coolant temperature T_c; and equivalence ratio Φ. The effects of each of these inputs on T_{exh} are studied and then they are compared with each other.

The variations in T_{exh} and the in-cylinder gas temperature (calculated using a recorded pressure trace and applying the ideal-gas law for a closed engine cycle) with increasing intake pressure are shown in Fig. 3 (the ON, engine speed, intake temperature, equivalence ratio, and coolant temperature are held constant). The higher intake pressure in Fig. 3(a) results in earlier and shorter ignitions close to the top dead centre (TDC), which

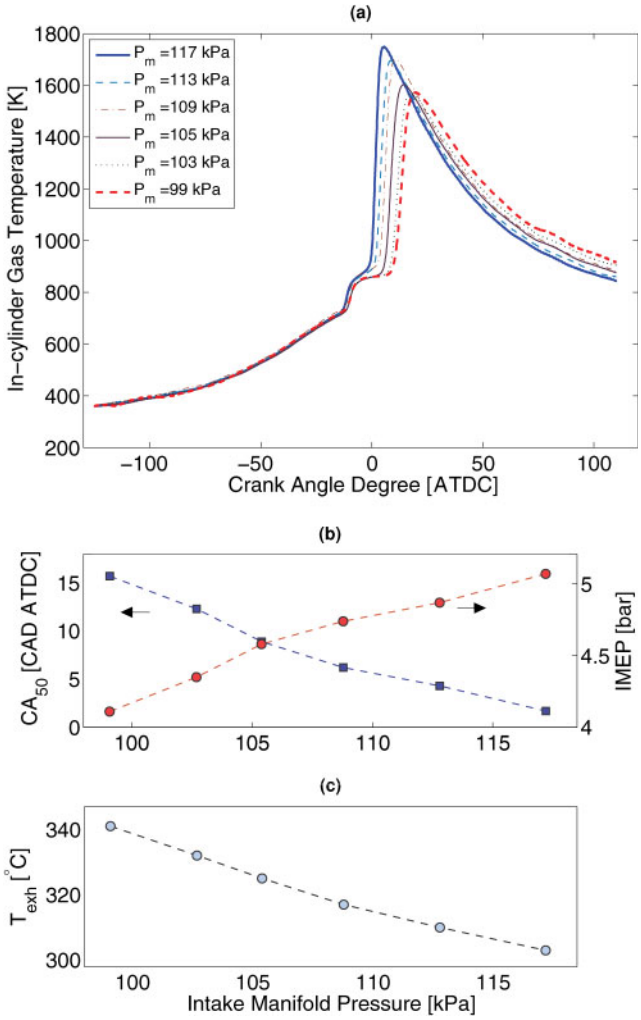

Fig. 3 Variations in the HCCI exhaust and in-cylinder temperatures with the intake pressure (fuel, PRF 0; $N = 1016$ r/min; $\Phi = 0.44$; $T_m = 87.3$ °C; data points 81 to 86 in Appendix 2). In this and subsequent figures, CAD means degrees CA

leads to a higher peak temperature but a lower cylinder temperature during the expansion stroke. CA_{50} in Fig. 3 advances from 15.7° CA ATDC to 1.7° CA ATDC as the intake pressure increases by 18 kPa (points 81 to 86 in Appendix 2). When the ignition is delayed, most of the energy is released part of the way down the expansion stroke and this increases the exhaust temperature. T_{exh} decreases by 38 °C when the intake pressure is increased from 99 kPa to 117 kPa ($\Delta T_{exh}/\Delta P_m = -2.1$ °C/kPa). This is mainly caused by advancing the HCCI combustion when the intake pressure is increased. As expected, the IMEP increases by boosting the intake pressure in Fig. 3. However, T_{exh} decreases with increasing engine load (IMEP) at a fixed-equivalence-ratio fuelling condition. The results in Fig. 3 combined with the CA_{50} values in Appendix 2 show that T_{exh} is strongly influenced by the HCCI ignition timing location.

The variation in T_{exh} with fuel ON in Fig. 4 also shows that T_{exh} is very dependent on CA_{50}. T_{exh} increases by 20 °C as the ON is increased from 22 to 40 ($\Delta T_{exh}/\Delta ON = +1.1$ °C/ON). In the transient HCCI test in Fig. 4, during a relatively constant-engine-load test condition, CA_{50} is delayed by about 8° CA as the ON is changed from 22 to 40. Increasing the ON increases the HCCI BD, as shown in Fig. 4(a), where the BD is doubled when the ON is increased by 18 units. (There is a strong coupling between CA_{50} and the BD, and the longer BD occurs at delayed CA_{50} after the TDC.) This leads to a prolonged heat release in the expansion stroke, which results in a higher T_{exh}. Delayed and longer heat release at a higher ON is also evident in Fig. 5 where two sample cycles from Fig. 4 are compared. In addition, the cyclic variation in CA_{50} (Fig. 4(a)) substantially increases when CA_{50} retards from 3° CA ATDC to 11° CA ATDC. This behaviour has been discussed in more detail in reference [**29**] for the Ricardo engine and it is mainly because the temperature rise from combustion is counteracted by the cooling from piston expansion when ignition retards and also because there is more thermally stratified charge which retards combustion.

The variations in T_{exh} versus two engine variables in Figs 3 and 4 represent two cases where the location of ignition timing (CA_{50}) is the main factor affecting T_{exh}. However, other factors can also play an important role when other engine variables such as the engine speed (Fig. 6), the coolant temperature (Fig. 7), and the intake temperature (Fig. 8) are changed. In Fig. 6, T_{exh} increases significantly from 315 °C to 418 °C when the engine speed increases

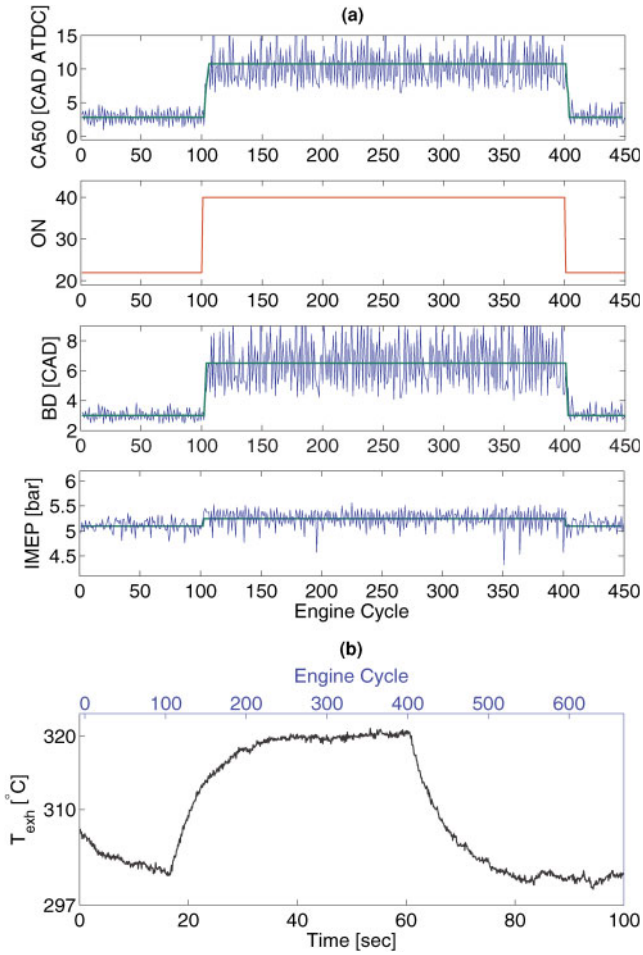

Fig. 4 Variation in the HCCI exhaust temperature with fuel ON (note the timescale of plot (b) in this figure starts before those of plots (a) and it ends after the last cycle of plots (a)) ($N = 815$ r/min; $\Phi = 0.44$; $P_m = 120$ kPa; $T_m = 117$ °C)

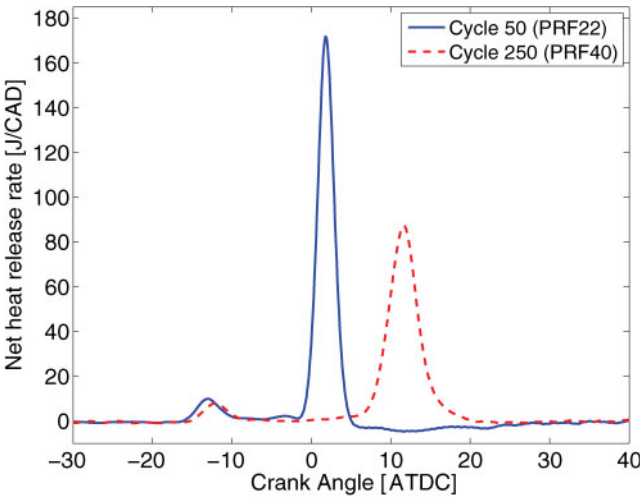

Fig. 5 Calculated net heat release rate for two sample cycles in Fig. 4

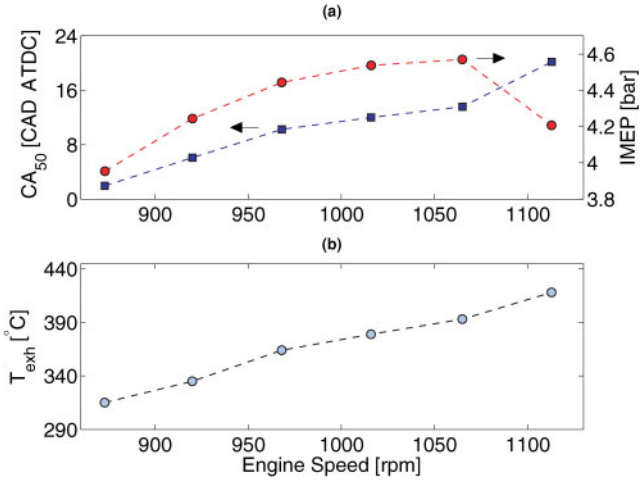

Fig. 6 Variation in the HCCI exhaust temperature with the engine speed (fuel, PRF 0; $\Phi = 0.56$; $P_m = 89$ kPa; $T_m = 91$ °C; data points 62 to 67 in Appendix 2)

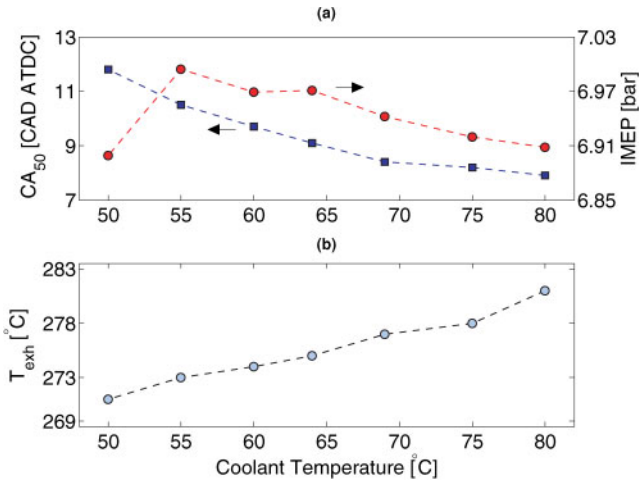

Fig. 7 Variation in the HCCI exhaust temperature with the coolant temperature (fuel, PRF 20; $N = 800$ r/min; $\Phi = 0.4$; $P_m = 119$ kPa; $T_m = 121$ °C; data points 157 to 163 in Appendix 2)

from 873 r/min to 1113 r/min ($\Delta T_{exh}/\Delta N = +4.3$ °C/10 r/min). This can be partly attributed to the change in the ignition timing, since CA_{50} retards from 1.9° CA ATDC to 20.2° CA ATDC (points 62 to 67 in Appendix 2). Changing the engine speed, in addition to varying the ignition timing, causes a large change in T_{exh}, since less heat loss is expected at higher engine speeds [**10**]. This becomes more important for late ignitions which have longer BDs [**29**] and for which there is more time available for heat loss. When the engine speed increases, there is both decreased heat loss and delayed ignition timing, and the two main compounding factors combine to have a significant influence on T_{exh}.

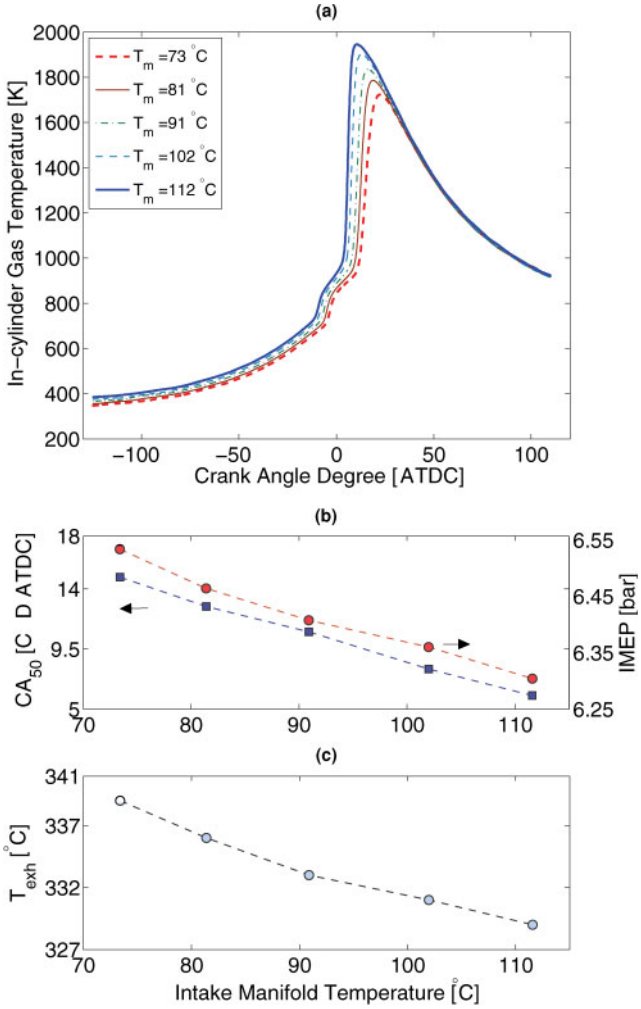

Fig. 8 Variations in the HCCI exhaust and in-cylinder temperatures with the intake temperature (fuel, PRF 10; $N = 997$ r/min; $\Phi = 0.42$; $P_m = 120$ kPa; data points 96 to 100 in Appendix 2)

The variation in T_{exh} versus the coolant temperature in Fig. 7 shows another example where the heat loss plays an important role in addition to the ignition timing location. Decreasing the coolant (wall) temperature results in a higher heat loss and retards HCCI combustion. In Fig. 7, CA_{50} retards from 7.9° CA ATDC to 11.8° CA ATDC when T_c decreases from 80 °C to 50 °C; thus, T_{exh} is expected to increase. However, T_{exh} decreases from 281 °C to 271 °C ($\Delta T_{exh}/\Delta T_c = +0.3$ °C/°C). This indicates that the impact from the heat loss factor is stronger and opposite to that of the ignition timing location in Fig. 7. When the coolant temperature decreases, there is both increased heat loss and delayed ignition timing; two main opposing factors combine to affect T_{exh}. This results in a moderate change in T_{exh}, although the coolant temperature is substantially changed in Fig. 7.

Similarly, a moderate 10 °C decrease in T_{exh} despite a large intake temperature change from 73 °C to 112 °C is shown in Fig. 8 with a slope $\Delta T_{exh}/\Delta T_m = -0.3$ °C/°C. Concurrently, CA_{50} advances significantly from 14.9° CA ATDC to 6.0° CA ATDC during the increase in the intake temperature (points 96 to 100 in Appendix 2). Similar to the results in Figs 6 and 7, this indicates that there is another factor besides CA_{50} which influences T_{exh}. The second main factor is that a higher initial temperature (energy input air) at higher T_m conditions leads to a higher in-cylinder gas temperature for most of the engine cycle, as shown in Fig. 8(a). This factor acts contrary to the changing ignition timing when the intake temperature is varied; thus, the variation in T_{exh} with the intake temperature in Fig. 8 is not as large as those seen in Figs 3 to 6.

The influence of the equivalence ratio on T_{exh} is shown in Fig. 9. T_{exh} increases by 17 °C when Φ increases from 0.36 to 0.43. CA_{50} advances 10.5° with increasing equivalence ratio. Thus, T_{exh} increases when a higher Φ is used despite advancing the HCCI combustion towards the TDC. This trend is opposite to what is observed in Figs 3 to 6 and Fig. 8. Two opposing factors affecting T_{exh} are present in Fig. 9 (similar to those affecting T_c in Fig. 7 and those affecting T_m in Fig. 8). The two opposing factors here are the ignition timing location and the injected fuel energy content. More energy is released when the fuel mass flowrate in the intake charge increases under a constant-air-mass-flowrate condition (higher Φ). Here, the influence from the second factor, namely the energy input fuel, on T_{exh} is stronger than that of the ignition timing location. This is

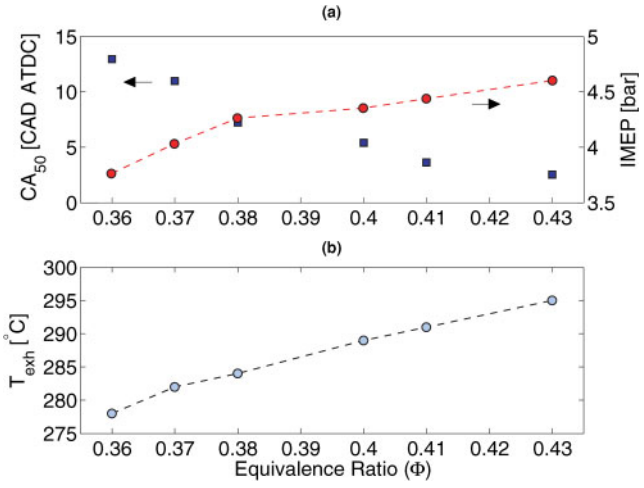

Fig. 9 Variation in the HCCI exhaust temperature with the equivalence ratio (fuel, PRF 0; $N = 900$ r/min; $P_m = 110$ kPa; $T_m = 92$ °C; data points 51 to 56 in Appendix 2)

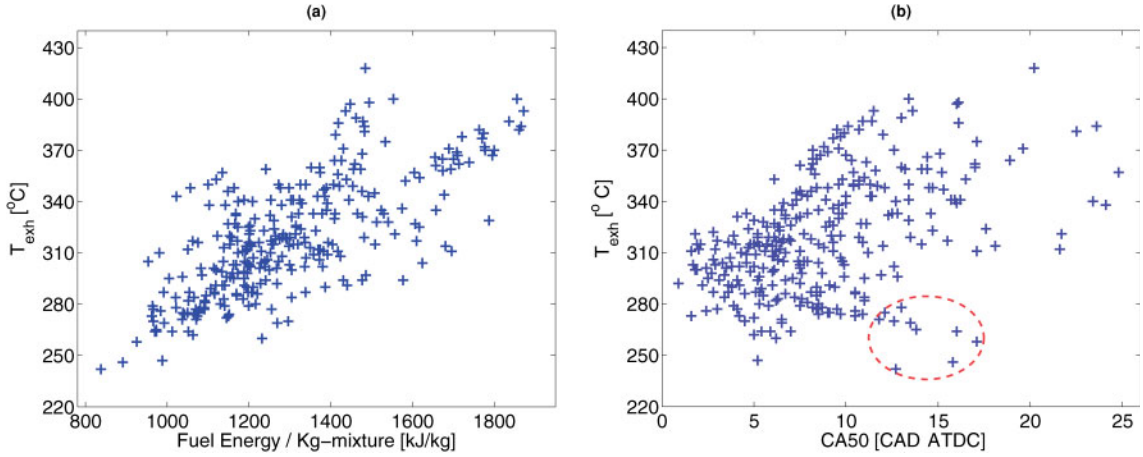

Fig. 10 Variation in the HCCI exhaust temperature with CA50 and specific fuel energy of the mixture

opposite to the results in Fig. 8 where the influence from the ignition timing location is stronger than that of the second factor, namely the input air temperature.

The variation in T_{exh} with CA_{50} and the specific energy input fuel is plotted in Fig. 10 for all the 304 steady state HCCI data points used in this study. The overall trend in Fig. 10 is consistent with observations from previous figures and suggests an increase in T_{exh} by retarding CA_{50} or increasing the energy input fuel per mass of the air–fuel mixture. Variations from the overall trend in Fig. 10 are due to the diversity of operating conditions where the other inputs are also varied (see Table 2). For instance the dashed ellipse in Fig. 10(b) consists of data points with either a low coolant temperature ($T_c \leqslant 67\,^{\circ}C$) or an ultra-lean mixture ($\Phi \leqslant 0.36$) (data points 51, 118–120, 132, 134, 149, 163, 195 and 196 in Appendix 2). The results in Figs 9 and 10 indicate the possibility that the slope of T_{exh} could change sign when Φ is increased. This behaviour is in fact measured and shown in Fig. 11. T_{exh} first increases with increasing Φ but then begins to decrease when the intake charge is made richer than $\Phi = 0.48$. The increase in Φ from 0.43 to 0.5 results in advancing CA_{50} from 12° CA ATDC to 2.9° CA ATDC (points 44 to 50 in Appendix 2). As CA_{50} approaches the TDC in Fig. 11, the effect of the variation in the ignition timing location (the first factor) finally overcomes the effect from changes in the fuel energy content (the second factor). Data points 38–43 in Appendix 2 exhibit another example of concave-down behaviour in T_{exh} versus Φ.

Table 3 summarizes the results of comparing the effects of six engine variables on T_{exh} in HCCI conditions. The first group are the primary inputs for which the location of ignition timing is the main factor that influences T_{exh}. This group includes the intake pressure and the fuel ON. As discussed, later and longer ignitions TDC result in hotter exhaust gases. The second group are compounding inputs which include the engine speed. Variation in the heat loss of the exhaust gases is the second main factor which is coupled with the factor of the ignition timing location to amplify the influence of the engine speed on T_{exh}. The third group are inputs that cause opposing effects. The coolant temperature, the intake temperature, and the equivalence ratio are in this group. In this case, the final trend of the variation in T_{exh} depends on whether the influence of the ignition timing location is stronger or weaker than the second main factor (the heat loss, the energy input air, or the energy input fuel).

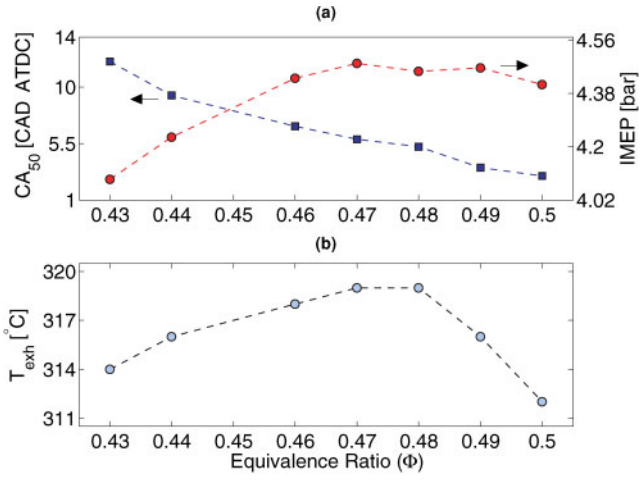

Fig. 11 Variation in the HCCI exhaust temperature with equivalence ratio (fuel, PRF 0; $N = 900$ r/min, $P_m = 100$ kPa; $T_m = 89\,^{\circ}C$; data points 44 to 50 in Appendix 2)

Table 3 Trend of variation in the HCCI exhaust temperature with the six main engine variables

Variable	T_{exh}	Main effect	Slope $\Delta T_{exh}/\Delta x$
Intake pressure P_m ↑	↓	One	−2.1 °C/kPa
ON ↑	↑	One	+1.1 °C/ON
Engine speed N ↑	↑	Two parallel	+4.3 °C/10 r/min
Coolant temperature T_c ↑	↑ / ↓	Two opposing	+0.3 °C/°C
Intake temperature T_m ↑	↑ / ↓	Two opposing	−0.3 °C/°C
Equivalence ratio Φ ↑	↑ / ↓	Two opposing	Variable

The steady state experimental data are used to find an empirical correlation to provide understanding of the variations in T_{exh}. To simplify the correlation, a constant engine speed and constant coolant and oil temperatures are assumed. Two main parameters are selected to characterize T_{exh}: the specific energy input fuel (the magnitude parameter) and CA_{50} (the location parameter). The correlation found to work well for the experimental data is

$$T_{exh} = A_T + B_T \frac{q_f}{C_{V,mix}\ T_{ad,ave}} + C_T[\ln\ (CA_{50})]^2 \qquad (1)$$

where q_f is the specific energy input fuel (kJ/kg) and CA_{50} is the CA for 50 per cent burned fuel (deg CA ATDC). $C_{V,mix}$ is the constant-volume specific heat of the air–fuel mixture (kJ/kg K) and $T_{ad,ave}$ is the average constant-volume adiabatic flame temperature. The specific heat and the adiabatic flame temperature are calculated at constant volume since the HCCI cycle is a closer approximation to constant-volume combustion than to constant-pressure combustion. The constant-volume adiabatic flame temperature is calculated for all HCCI experimental data. This yields $T_{ad,ave} = 1950$ K. Half of the 304 HCCI experimental data are used to parameterize the correlation (1) and the resulting values of the constants are $A_T = 160.75$, $B_T = 142.42$, and $C_T = 7.25$. Predicted T_{exh} values are compared with those from experiments in Fig. 12 for all 304 HCCI operating conditions used in this study. The results indicate that the simple correlation captures the trend of T_{exh} variations, showing good agreement with the experimental data for the majority of operating conditions. An uncertainty of ±23.7 °C is found in the predictions from equation (1). (The uncertainty is determined by 2σ, where σ is the standard deviation of residual errors. This means that the true value, with 95 per cent confidence, lies within $\pm 2\sigma$ of the estimated value [**35**].) The main source of error in Fig. 12 comes from ignoring the heat loss variations in correlation (1) for the data points with variable engine speed or variable coolant temperature (see Table 2). Equation (1) is also tested for a different

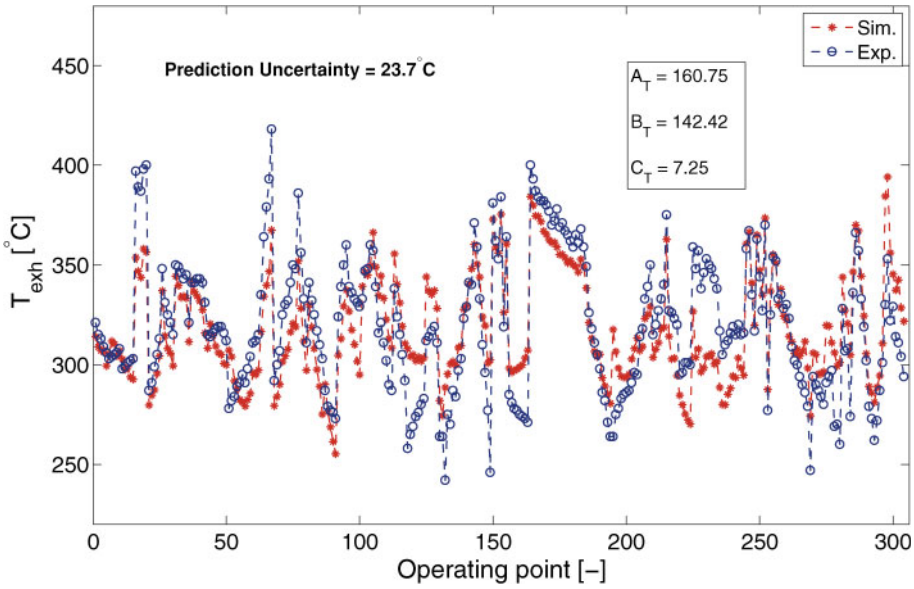

Fig. 12 Comparison between the predicted (i.e. simulation (Sim.)) and the experimental (Exp.) T_{exh} for four PRF blends in different HCCI steady state engine conditions (fuel PRF values, 0, 10, 20, and 40)

engine with the configuration listed in Table 4. Figure 13 shows the comparison between the measured exhaust temperatures and predictions from the equation (1) for 43 different HCCI operating points from the new engine. The results indicate an uncertainty of $\pm 4.1\,^{\circ}$C in the exhaust temperature predictions. The smaller prediction uncertainty in Fig. 13 than in Fig. 12 is due to the constant-engine-speed and constant-coolant-temperature operating conditions for the engine in Table 4. Overall, correlation (1) can predict the exhaust temperature for the two different engines with an uncertainty of less than $\pm 24\,^{\circ}$C and is simple and computationally efficient. This correlation can be useful for model-based control of the exhaust temperature in HCCI engines, particularly when the feedback from the exhaust temperature sensor can be utilized to modify the model predictions. Since correlation (1) considers only the two main factors influencing T_{exh}, a more extensive model may be required if targets other than exhaust temperature control are intended.

Table 4 Configurations of the Mercedes head engine (ABDC, after bottom dead centre)

Parameter (units)	Value
Bore (mm)	97
Stroke (mm)	88.9
Compression ratio	12
Displacement (l)	0.657
Number of valves	4
Intake valve opening (deg CA ABDC)	−170
Intake valve closing (deg CA ABDC)	40
Exhaust valve opening (deg CA ABDC)	−62
Exhaust valve closing (deg CA ABDC)	148

Comparing the trends of the variations in T_{exh} with engine load (IMEP) in Figs 3, 6 to 9, and 11 indicates that T_{exh} is not necessarily a function of the engine load in the HCCI engine. In Fig. 3, T_{exh} decreases with increasing engine load, but T_{exh} increases with increasing engine load in Fig. 8. (When the intake manifold temperature increases in Fig. 7, the amount of intake charge drops, which causes a decrease in the IMEP.) Similarly, T_{exh} increases in Figs 6 and 7 irrespective of the engine load increase or decrease. This is because T_{exh} is mainly a function of the other discussed variables that may also influence the engine load. However, the IMEP in the HCCI mode mainly depends on the fuelling rate rather than on the ignition timing, but the IMEP becomes strongly dependent on the ignition timing for conditions that have a constant fuelling rate [**29**]. This explains why the IMEP increases in Figs 3 and 8 with either increasing intake pressure or decreasing intake temperature. Since Φ is kept constant in Figs 3 and 8, a higher intake pressure and lower intake temperature require higher fuel mass flow-rates. However, the IMEP decreases for late ignition even if the fuelling rate is increased. This is evident for the data point at 1113 r/min (data point 67 in Appendix 2) in Fig. 6 with $CA_{50} = 20.2^{\circ}$ CA ATDC for which the IMEP drops despite the increasing fuelling rate. (To keep Φ constant with increasing engine speed, the fuelling rate is increased in proportion to the increased air into the engine. The air mass

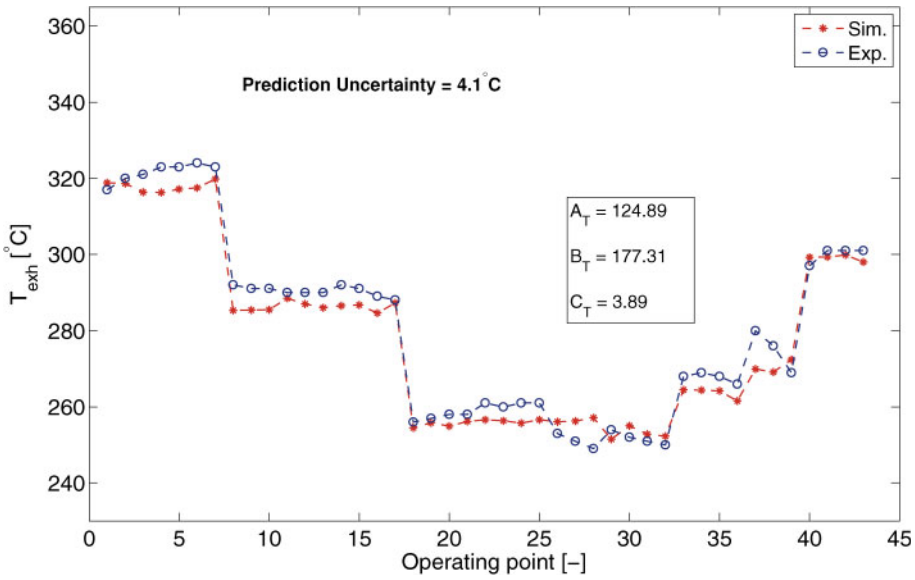

Fig. 13 Comparison between the predicted (i.e. simulation (Sim.)) and the experimental (Exp.) T_{exh} for different HCCI steady state operating points of the Mercedes head engine (fuel, PRF 0; $N = 1025$ r/min; $\Phi = 0.34$–0.48; $P_m = 89$–120 kPa; $T_m = 79$–$82\,^{\circ}$C)

flowrate for the data points in Fig. 6 increases from 2.3 g/s to 3.2 g/s with increasing engine speed from 813 r/min to 1113 r/min.)

The CO and HC emissions for the data points from the P_m sweep (Fig. 3), N sweep (Fig. 6), T_m sweep (Fig. 8), and Φ sweep (Fig. 11) are shown in Fig. 14. A strong relation is observed between CA_{50} and the amounts of the CO and HC emissions. This relation holds for all the four engine input variables. Both CO and HC emissions increase with increasing CA_{50}. A higher in-cylinder temperature during HCCI combustion tends to occur for CA_{50} at earlier ignitions, as shown in Figs 3(a) and 8(a). A high combustion temperature which is well characterized by the peak cylinder cycle temperature is the main requirement for CO and HC oxidation in HCCI engines [**1**, **3**, **5**]. However, a higher peak combustion temperature at earlier ignitions also causes higher NO_x emissions. This is evident in the NO_x values in the N sweep data points (data points 62 to 67 in Appendix 2) where NO_x increases from 0 ppm to 144 ppm when CA_{50} advances from 20.2° CA aTDC to 1.9° CA aTDC.

3.2 Variations in T_{exh} for the SI mode versus the HCCI mode

Switching between the HCCI and SI modes is a technique to increase the limited engine output power in HCCI by switching to the SI mode to obtain full power. These two combustion modes have different T_{exh} characteristics due to the different combustion principles. The ignition timing location is an important factor in both combustion modes. Ignition timing in an SI engine is adjusted by the spark timing, while the engine operating conditions determine the ignition timing (CA_{50}) in the HCCI mode. This leads to less complicated behaviour in T_{exh} variations in the SI mode than in the HCCI mode. The spark timing, engine speed, and load are the three main factors that influence T_{exh} in the SI mode [**10**]. Similar to HCCI, later ignitions result in higher exhaust temperatures; this is also used as a technique to reduce catalyst light-off time during a cold start [**36**]. Experimental results for the SI mode in the fixed-ignition-timing (CA_{50}) condition as the engine speed and intake pressure are varied for stoichiometric operation are shown in Fig. 15(a). Similar to the results in Fig. 6, T_{exh} also increases in the SI mode when the engine speed increases. However, opposite to what was observed in the HCCI mode (Fig. 3), T_{exh} increases with increasing intake pressure. As shown in Fig. 15(b), increasing the engine load in the SI mode by boosting the intake pressure leads to increasing T_{exh}. This is different from that of the HCCI mode for which the engine load is not a main factor affecting T_{exh}. In addition, results from 36 different operating points in Fig. 15 show that the engine speed has a larger impact on T_{exh} in the SI mode than does the intake pressure or the engine load ($\Delta T_{exh}/\Delta N = 1.2$–$1.3$ °C/10 r/min; $\Delta T_{exh}/\Delta P_m = 0.5$–$0.7$ °C/kPa; $\Delta T_{exh}/\Delta IMEP = 0.04$–$0.07$ °C/kPa). The impact of the engine speed on T_{exh} in the SI mode can be significantly larger than that of the engine load as seen by comparing the typical range of variations in the engine speed with that in the engine load or intake pressure in SI engines. A similar trend is also observed in the HCCI mode where the engine speed has more influence on T_{exh} than does the intake pressure.

Finally, the transient exhaust temperature T_{exh} during the HCCI–SI mode switching at nearly

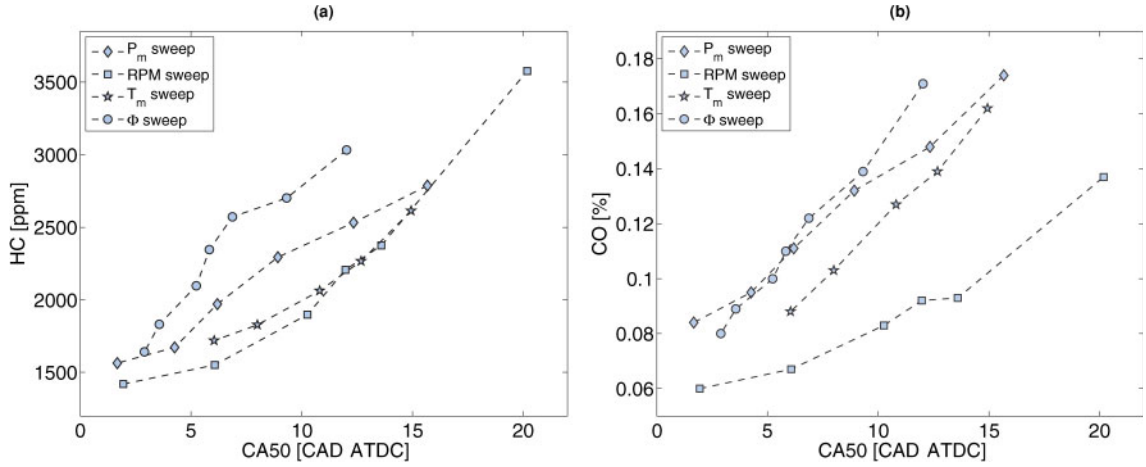

Fig. 14 Variations in the HC and CO emissions with four engine variables: first, a P_m sweep from Fig. 3; second, a speed (labelled RPM) sweep from Fig. 6; third, a T_m sweep from Fig. 8; fourth, a Φ sweep from Fig. 11

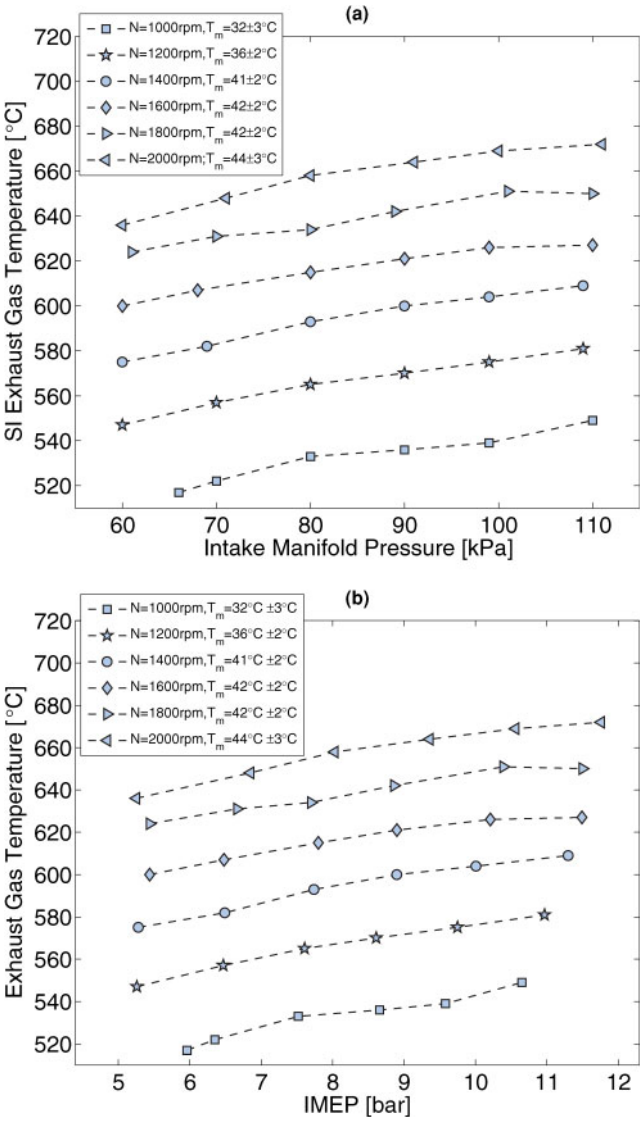

Fig. 15 Variation in the exhaust temperature in the SI mode with engine load and engine speed

constant load is shown in Fig. 16. The exhaust gas temperature is substantially higher in the SI mode than in the HCCI mode for the constant-load condition. The BD in the SI mode is five times that in the HCCI mode for the test condition in Fig. 16 ($BD_{HCCI} = 4^\circ$ CA; $BD_{SI} = 20^\circ$ CA). Longer combustion in SI results in the release of more energy at later CAs compared with the HCCI results and causes in a higher T_{exh} in the SI mode. In addition, the SI mode typically runs with significantly richer intake charge than does the HCCI mode; note that the fuel conversion efficiency in the SI mode is lower than in the HCCI mode. For instance the value of Φ changes from 0.45 to 0.95 when the Ricardo engine is switched from the HCCI mode to the SI mode in Fig. 16. The richer mixture requirement in the SI mode can cause a substantial increase in T_{exh} as

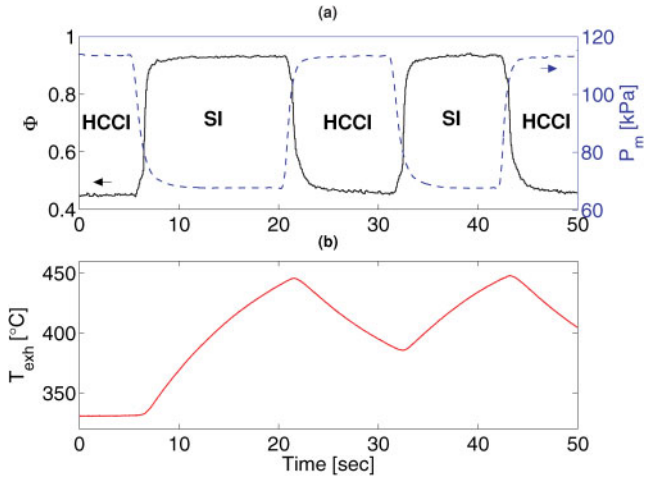

Fig. 16 Variation in the exhaust gas temperature during the HCCI–SI mode switching with similar steady state loads ($CA_{50} = 7.4 \pm 2.2^\circ$ CA ATDC; $N = 1000$ r/min; $T_m = 98.3 \pm 1.2$ °C; IMEP $= 4.6 \pm 0.4$ bar where the coefficients of variation in the IMEP in the SI mode and the HCCI mode are about 1.1 per cent and 2.2 per cent respectively)

more heat is released compared with that in the HCCI mode. For almost the same load condition in Fig. 16 the amount of heat released increases by about 50 J when the Ricardo engine switches from the HCCI mode to the SI mode. The higher heat released (460 J) in the SI mode in Fig. 16 contributes to a higher T_{exh} in the SI mode than in the HCCI mode. Since the mode switching from HCCI to SI is usually from a medium-load to a full-load condition in order to extend the HCCI operating range, T_{exh} should substantially increase during the mode switching from HCCI to the SI at a higher engine load. This is also evident from comparing the results in Fig. 3 with those in Fig. 15 where a significantly higher T_{exh} is observed in the high-load SI conditions in Fig. 15 compared with the medium-load HCCI conditions in Fig. 3.

4 SUMMARY AND CONCLUSIONS

The variations in the HCCI exhaust gas temperature are studied as this is an essential step in understanding the effects of different engine variables on T_{exh}. Over 340 steady state and transient experimental operating points from a single-cylinder port fuel injection engine with zero valve overlap period are used to investigate T_{exh} as a function of several main engine variables. The analysis of experimental measurements results in the following findings for the engines studied.

1. A large number (92 points) of HCCI operating conditions have T_{exh} lower than the typical catalyst light-off temperature (300 °C). All points with low T_{exh} have negligible NO_x emission while having a minimum IMEP of about 4 bar. These data points represent potential desirable HCCI points but the low T_{exh} is detrimental to catalyst operation for converting HC and CO emission in these conditions.
2. The variation in T_{exh} in the HCCI mode can be explained by a combination of different factors, as summarized in Fig. 17. T_{exh} in the HCCI mode depends on the location of ignition timing which is determined by a combination of factors from different engine variables, as seen in Fig. 17. In addition to the ignition timing (the main factor), T_{exh} is influenced by other secondary factors including the heat loss, energy input air, energy input fuel, and BD. A conflict between the primary factor and secondary factors leads to a complex behaviour in the variations in T_{exh} in HCCI mode. The engine variables are divided into three different groups: primary, compounding, and opposing variables. The intake pressure and fuel ON are the primary variables for which the location of ignition timing (CA_{50}) is the dominant factor. For these variables T_{exh} increases with increasing CA_{50}. The engine speed is a compounding variable, and the coolant temperature, intake temperature, and equivalence ratio are opposing variables. T_{exh} increases substantially with increasing engine speed since CA_{50} increases (first factor) and the engine heat loss (second factor) is reduced. However, T_{exh} can either increase or decrease when Φ increases. This depends on the competition between the location of heat release with advancing CA_{50} (first factor, decreasing T_{exh}) and the increasing amount of heat released with increasing energy input fuel (second factor, increasing T_{exh}) when Φ increases.
3. The variations in T_{exh} can be predicted for constant-engine-speed and constant-coolant-temperature conditions by using a simple empirical correlation that incorporates two input parameters: the specific energy input fuel (the magnitude parameter) and CA_{50} (the location parameter). The empirical correlation could predict T_{exh} for two different engines for a total of 347 HCCI operating points with an uncertainty of less than ± 24 °C.
4. CO and HC emissions in HCCI are strongly dependent on the location of ignition timing (CA_{50}). This relation appears to be independent of the four engine variables (P_m, N, T_m, and Φ) studied. Higher CO and HC emissions are observed when shifting CA_{50} from early ignitions to late ignitions after TDC. This is because of the higher peak in-cylinder temperature during combustion when ignition occurs close to the TDC. NO_x emission shows the opposite trend where NO_x increases when CA_{50} is advanced towards the TDC.
5. Studying the variation in T_{exh} with the engine load (IMEP) did not support a correlation existing between T_{exh} and the engine load in the HCCI mode. This indicates that T_{exh} in the HCCI mode is not a main function of the engine load. This is different from the SI mode where the engine load is one of the three main factors affecting T_{exh}.
6. Similar to the SI mode, T_{exh} in the HCCI mode increases with increasing engine speed when other

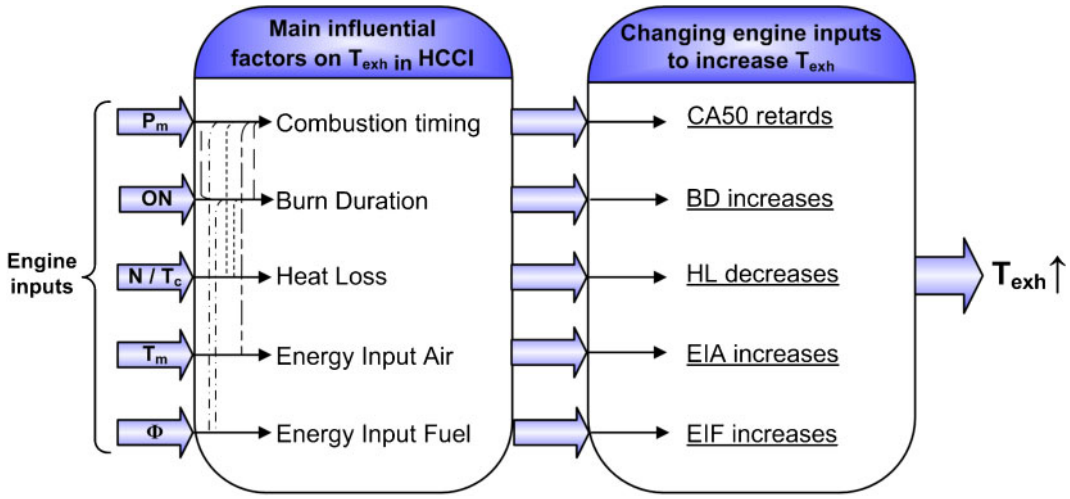

Fig. 17 Schematic diagram of the different factors influencing the HCCI exhaust temperature (HL, heat loss; EIA, energy input air; EIF, energy input fuel)

variables are held constant. However, opposite to the SI mode, T_{exh} in the HCCI mode increases with decreasing intake pressure. In both modes, the variation in the engine speed has a larger impact on T_{exh} than does the intake pressure.

7. T_{exh} in the HCCI mode is significantly lower than in the SI mode for a similar engine load (IMEP) condition. Shorter BD and lower fuel energy content in the HCCI mode lead to a lower T_{exh} than that in the SI mode under a similar load condition.

ACKNOWLEDGEMENTS

The authors acknowledge the Natural Sciences and Engineering Research Council of Canada and AUTO21 Network of Centers of Excellence and Daimler for supporting this work. For their contributions in collecting the experimental data, R. Lupul and A. Audet are gratefully acknowledged.

REFERENCES

1 **Zhao, H.** *Homogeneous charge compression ignition (HCCI) and controlled auto ignition (CAI) engines for the automotive industry*, 2007 (CRC Press, Boca Raton, Florida).

2 **Zhao, F., Asmus, T. W., Assanis, D. N., Dec, J. E., Eng, J. A.,** and **Najt, P. M.** *Homogeneous charge compression ignition (HCCI) engines,* SAE Publication PT-94, 2003 (SAE International, Warrendale, Pennsylvania).

3 **Stanglmaier, R. H.** and **Roberts, C. E.** Homogeneous charge compression ignition (HCCI): benefits, compromises, and future engine applications. SAE paper 1999-01-3682, 1999.

4 Homogeneous charge compression ignition technology – a report to the U.S. congress. Technical Report, US Department of Energy, Washington, DC, USA, 2001.

5 **Sjöberg, M.** and **Dec, J. E.** An investigation into lowest acceptable combustion temperatures for hydrocarbon fuels in HCCI engines. *Proc. Combust. Inst.*, 2005, **30**, 2719–2726.

6 **Dec, J. E.** A computational study of the effects of low fuel loading and EGR on heat release rates and combustion limits in HCCI engines. SAE paper 2002-01-1309, 2002.

7 **Aceves, S., Flowers, D., Espinoza-Loza, F., Martinez-Frias, J., Dibble, R., Christensen, M., Johansson, B.,** and **Hessel, R. P.** Piston-liner crevice geometry effect on HCCI combustion by multizone analysis. SAE paper 2002-01-2869, 2002.

8 **Lu, X., Chen, W., Hou, Y.,** and **Huang, Z.** Study on the ignition, combustion and emissions of HCCI combustion engines fueled with primary reference fuels. SAE paper 2005-01-0155, 2005.

9 **Wanker, R. J., Wurzenberger, J. C.,** and **Schuemie, H. A.** Three-way catalyst light-off during the NEDC test cycle: fully coupled 0D/1D simulation of gasoline combustion, pollutant formation and aftertreatment systems. SAE paper 2008-01-1755, 2008.

10 **Heywood, J. B.** *Internal combustion engine fundamentals*, 1988 (McGraw-Hill, New York).

11 **Ferrari, V., Rabinowitz, H., Siemund, S., Collinq, T.,** and **Campbell, B.** Achieving EURO III and EURO IV with ultra-low precious metal loadings. SAE paper 2007-01-2565, 2007.

12 **Jean, E., Leroy, V., Montenegro, G., Onorati, A.,** and **Laurell, M.** Impact of ultra low thermal inertia manifolds on emission performance. SAE paper 2007-01-0935, 2007.

13 **Tanikawa, K., Hirota, T., Yamada, T., Komori, M., Zhang, G.,** and **Muraki, H.** Development of advanced three-way catalyst technology. SAE paper 2008-01-1645, 2008.

14 **Williamson, W. B., Dou, D.,** and **Robota, H. J.** Development of advanced three-way catalyst technology. SAE paper 1999-01-0776, 1999.

15 **Zinola, S., Lavy, J.,** and **Jaecker-Voirol, A.** Towards CO and HC aftertreatment devices for the next generation of diesel engines. SAE paper 2008-01-1543, 2008.

16 **Bhaskar, K., Sendilvelan, S.,** and **Jeyachandran, K.** Experimental investigation on cold start HC and CO emission control using electrically heated pre-catalyst (EHC) in Mark IV Ambassador SI engine. SAE paper 2004-28-0006, 2004.

17 **Oeser, P., Mueller, E.,** and **Haertel, G.** Novel emission technologies with emphasis on catalyst cold start improvements status report on VW–Pierburg burner/catalyst systems. SAE paper 940474, 1994.

18 **Borland, M.** and **Zhao, F.** Application of secondary air injection for simultaneously reducing converter-in emissions and improving catalyst light-off performance. SAE paper 2002-01-2803, 2002.

19 **Konstantinidis, P. A., Koltsakis, G. C.,** and **Stamatelos, A. M.** Computer aided assessment and optimization of catalyst fast light-off techniques. *Proc. IMechE, Part D: J. Automobile Engineering*, 1997, **211**(1), 21–37. DOI: 10.1243/0954407971526191.

20 **Bauer, H., Haldenwanger, H.-G., Hirth, P.,** and **Brück, R.** Thermal management of close coupled catalysts. SAE paper 1999-01-1231, 1999.

21 **Caraceni, A., Cioffi, V., Garofalo, F., Barberio, C.,** and **Saroglia, G.** Emission control technologies for EU stage IV+EOBD on small cars (Part I): prescreening of potential solutions. SAE paper 1999-01-0775, 1999.

22 **Williams, S., Hu, L., Nakazono, T., Ohtsubo, H.,** and **Uchida, M.** Oxidation catalysts for natural gas

engine operating under HCCI or SI conditions. SAE paper 2008-01-0807, 2008.
23 **Olsson, J., Haraldsson, G., Tunestål, P.,** and **Johansson, B.** A turbo charged dual fuel HCCI engine. SAE paper 2001-01-1896, 2001.
24 **Koopmans, L., Backlund, O.,** and **Denbratt, I.** Cycle to cycle variations: their influence on cycle resolved gas temperature and unburned hydrocarbons from a camless gasoline compression ignition engine. SAE paper 2002-01-0110, 2002.
25 **Sjöberg, M.** and **Dec, J. E.** An investigation of the relationship between measured intake temperature, BDC temperature, and combustion phasing for premixed and DI HCCI engines. SAE paper 2004-01-1900, 2004.
26 **Santoso, H., Matthews, J.,** and **Cheng, W. K.** Managing SI/HCCI dual-mode engine operation. SAE paper 2005-01-0162, 2005.
27 **Figliola, R. S.** and **Beasley, D. E.** *Theory and design for mechanical measurements*, 2000 (John Wiley, New York).
28 **Lupul, R.** *Steady state and transient characterization of a HCCI engine with varying octane fuel.* MSc Thesis, University of Alberta, Edmonton, Alberta, Canada, 2008.
29 **Shahbakhti, M.** and **Koch, C. R.** Characterizing the cyclic variability of ignition timing in an HCCI engine fueled with *n*-heptane/iso-octane blend fuels. *Int. J. Engine Res.*, 2008, **9**(5), 361–397. DOI: 10.1243/14680874JER01408.
30 **Kirchen, P., Shahbakhti, M.,** and **Koch, C. R.** A skeletal kinetic mechanism for PRF combustion in HCCI engines. *J. Combust. Sci. Technol.*, 2007, **179**, 1059–1083.
31 **Rassweiler, G. M.** and **Withrow, L.** Motion pictures of engine flames correlated with pressure cards. *SAE Trans.*, 1938, **42**(5), 185–204.
32 **Audet, A.** *Closed loop control of HCCI using camshaft phasing and dual fuels.* MSc Thesis, University of Alberta, Edmonton, Alberta, Canada, 2008.
33 **Shahbakhti, M.** and **Koch, C. R.** Dynamic modeling of HCCI combustion timing in transient fueling operation. SAE paper 2009-01-1136, 2009.
34 **Millo, F.** and **Ferraro, C. V.** Knock in S.I. engines: a comparison between different techniques for detection and control. SAE paper 982477, 1998.
35 **Moffat, R. J.** Describing the uncertainties in experimental results. *Expl Thermal Fluid Sci.*, 1988, **1**, 3–17.
36 **Russ, S., Thiel, M.,** and **Lavoie, G.** SI engine operation with retarded ignition: part 2 – HC emissions and oxidation. SAE paper 1999-01-3507, 1999.

APPENDIX 1

Notation

ABDC	after bottom dead centre
AFR	air-to-fuel ratio
ATDC	after top dead centre
BD	burn duration
CA	crank angle
CA_{50}	crank angle for 50 per cent burned fuel
CO	carbon monoxide
CO_2	carbon dioxide
ECU	engine control unit
EGR	exhaust gas recirculation
HC	hydrocarbon
HCCI	homogeneous charge compression ignition
IMEP	indicated mean effective pressure
NO_x	nitrogen oxides
ON	octane number
PRF	primary reference fuel
SI	spark ignition
TDC	top dead centre
THC	total hydrocarbon

APPENDIX 2

Summary of steady state HCCI experiments

Data points 1–95 use PRF 0 fuel, points 96–100 use PRF 10 fuel, points 101–163 use PRF 20 fuel, and points 164–304 use PRF 40 fuel.

	Engine operating conditions								Engine emissions		
Data point	N (r/min)	Φ	P_m (kPa)	T_m (°C)	EGR (%)	T_{exh} (°C)	CA50 (deg CA)	IMEP (bar)	CO (%)	HC (ppm)	NO_x (ppm)
1	810	0.50	101	82	0	321	7.7	4.9	0.09	2839	1
2	810	0.52	101	82	0	315	5.7	4.9	0.07	2441	2
3	810	0.53	101	82	0	313	4.7	4.9	0.07	2414	2
4	810	0.53	101	82	0	309	4.6	4.9	0.06	2170	16
5	810	0.54	101	82	0	306	2.8	4.8	0.06	2221	19
6	810	0.45	101	92	0	303	7.5	4.5	0.12	2905	1
7	810	0.46	101	91	0	304	8.5	4.5	0.11	2789	1
8	810	0.47	101	91	0	305	7.9	4.6	0.11	2810	1
9	810	0.48	101	92	0	306	6.3	4.7	0.10	2789	1
10	810	0.49	101	93	0	308	6.1	4.7	0.09	2653	1
11	810	0.44	101	102	0	298	7.6	4.3	0.13	2967	1
12	810	0.45	101	103	0	299	6.0	4.4	0.12	2861	1
13	809	0.47	101	102	0	301	5.5	4.5	0.10	2612	1
14	810	0.49	101	102	0	302	4.2	4.6	0.09	2606	1
15	810	0.51	101	102	0	303	2.9	4.6	0.07	2344	4
16	1193	0.56	102	100	0	397	16.0	5.2	0.12	3341	2
17	1193	0.57	99	101	0	389	13.0	5.2	0.09	2586	4
18	1193	0.58	101	100	0	387	11.4	5.3	0.08	2411	5
19	1193	0.58	100	100	0	398	16.1	5.4	0.11	3070	2
20	1193	0.60	102	99	0	400	13.4	5.6	0.09	2812	5
21	810	0.42	110	100	0	287	3.6	4.6	0.11	2902	0
22	860	0.42	111	100	0	291	4.2	4.7	0.10	2760	0
23	908	0.42	110	102	0	299	4.8	4.7	0.11	2599	0
24	956	0.42	110	101	0	305	6.6	4.7	0.12	2677	0
25	1004	0.42	110	100	0	313	8.8	4.7	0.13	2776	0
26	908	0.49	90	100	0	348	14.7	4.0	0.12	2872	0
27	907	0.49	94	100	0	331	7.5	4.4	0.08	2029	1
28	908	0.49	98	101	0	325	5.7	4.5	0.07	1991	2
29	908	0.49	99	99	0	321	5.2	4.5	0.07	1988	3
30	908	0.49	101	100	0	315	4.0	4.6	0.06	1956	8
31	901	0.51	91	81	0	350	13.4	4.3	0.12	3035	0
32	901	0.52	90	81	0	349	10.4	4.4	0.10	2670	0
33	902	0.54	90	81	0	346	8.1	4.4	0.09	2237	4
34	901	0.54	91	81	0	343	7.9	4.4	0.08	1920	28
35	900	0.55	91	81	0	345	7.3	4.5	0.09	2104	19
36	900	0.57	91	82	0	321	1.8	4.1	0.07	1648	127
37	900	0.47	91	88	0	341	16.2	3.8	0.17	3510	0
38	899	0.48	91	88	0	341	13.4	4.0	0.13	3161	0
39	899	0.49	91	88	0	343	11.3	4.1	0.12	2953	0
40	899	0.50	90	87	0	343	10.0	4.2	0.11	2720	0
41	899	0.52	91	88	0	341	7.3	4.3	0.09	2285	0
42	899	0.55	91	88	0	331	4.1	4.2	0.08	1884	44
43	899	0.56	91	88	0	315	2.1	4.0	0.07	1541	144
44	901	0.43	100	90	0	314	12.0	4.1	0.17	3033	0
45	901	0.44	100	89	0	316	9.3	4.2	0.14	2702	0
46	901	0.46	101	87	0	318	6.9	4.4	0.12	2572	0
47	901	0.47	100	88	0	319	5.8	4.5	0.11	2346	0
48	901	0.48	100	89	0	319	5.2	4.5	0.10	2096	0
49	900	0.49	101	89	0	316	3.6	4.5	0.09	1832	1
50	900	0.50	101	89	0	312	2.9	4.4	0.08	1642	11
51	900	0.36	110	91	0	278	13.0	3.8	0.34	3108	0
52	900	0.37	111	92	0	282	11.0	4.0	0.32	3142	0
53	900	0.38	111	92	0	284	7.2	4.3	0.25	2939	0
54	900	0.40	110	92	0	289	5.4	4.4	0.15	2429	1
55	900	0.41	110	93	0	291	3.6	4.4	0.13	2175	3
56	900	0.43	110	92	0	295	2.5	4.6	0.12	2122	5
57	812	0.43	105	102	0	291	2.2	4.2	0.14	2288	8
58	872	0.43	105	102	0	298	2.7	4.2	0.11	2055	10
59	919	0.44	105	103	0	304	3.3	4.3	0.11	2040	7
60	967	0.43	105	103	0	311	5.6	4.3	0.11	2034	7
61	813	0.55	90	91	0	312	2.0	4.0	0.06	1521	129

	Engine operating conditions								Engine emissions		
Data point	N (r/min)	Φ	P_m (kPa)	T_m (°C)	EGR (%)	T_{exh} (°C)	CA50 (deg CA)	IMEP (bar)	CO (%)	HC (ppm)	NO_x (ppm)
62	873	0.55	89	92	0	315	1.9	4.0	0.06	1420	144
63	920	0.55	89	91	0	335	6.1	4.2	0.07	1551	81
64	968	0.56	89	91	0	364	10.3	4.4	0.08	1897	18
65	1016	0.56	89	91	0	379	12.0	4.5	0.09	2207	3
66	1065	0.56	89	92	0	393	13.6	4.6	0.09	2374	1
67	1113	0.56	89	91	0	418	20.2	4.2	0.14	3576	0
68	812	0.49	113	60	0	292	0.9	5.2	0.07	1517	14
69	873	0.48	113	60	0	300	1.8	5.3	0.07	1567	5
70	919	0.48	113	60	0	307	3.7	5.4	0.07	1452	7
71	968	0.48	114	62	0	325	6.4	5.6	0.09	1795	0
72	1016	0.48	113	60	0	330	6.7	5.6	0.10	1840	0
73	1064	0.49	113	61	0	332	6.7	5.7	0.09	1744	0
74	1112	0.48	113	63	0	341	8.9	5.6	0.10	1811	0
75	1161	0.48	114	64	0	350	9.6	5.6	0.12	2068	0
76	1160	0.48	113	65	0	348	9.0	5.6	0.11	1893	0
77	1017	0.54	88	93	0	386	16.1	4.2	0.11	2816	0
78	1016	0.54	93	91	0	356	8.3	4.5	0.08	1819	8
79	1017	0.54	95	93	0	333	4.6	4.4	0.07	1499	50
80	1016	0.54	98	93	0	311	1.6	4.2	0.06	1296	76
81	1016	0.45	99	88	0	341	15.7	4.1	0.17	2787	0
82	1016	0.44	103	88	0	332	12.3	4.4	0.15	2531	0
83	1016	0.44	105	87	0	325	8.9	4.6	0.13	2294	0
84	1016	0.44	109	88	0	317	6.2	4.7	0.11	1971	0
85	1016	0.44	113	86	0	310	4.3	4.9	0.10	1673	0
86	1016	0.45	117	87	0	303	1.7	5.1	0.08	1565	1
87	1016	0.38	119	89	0	287	8.6	4.6	0.25	2358	0
88	1016	0.37	124	90	0	279	5.8	4.7	0.20	2049	1
89	1016	0.37	127	89	0	277	4.1	4.9	0.17	1899	1
90	1016	0.37	128	92	0	276	2.4	4.9	0.15	1798	2
91	1016	0.37	131	94	0	273	1.6	5.0	0.15	1754	3
92	1016	0.51	99	95	0	324	4.7	4.4	0.07	1550	3
93	1016	0.51	99	95	0	339	6.6	4.6	0.09	1816	2
94	1015	0.51	99	94	0	350	10.7	4.7	0.10	2338	1
95	1015	0.51	99	96	0	360	13.0	4.8	0.14	3342	2
96	997	0.42	120	73	0	339	14.9	6.5	0.16	2613	0
97	997	0.41	120	81	0	336	12.7	6.5	0.14	2267	0
98	997	0.41	120	91	0	333	10.8	6.4	0.13	2062	0
99	997	0.42	120	102	0	331	8.0	6.4	0.10	1827	0
100	997	0.42	120	112	0	329	6.0	6.3	0.09	1719	0
101	1053	0.49	111	105	0	333	12.8	7.4	0.06	2376	10
102	1101	0.49	112	105	0	347	15.3	7.6	−0.00	502	6
103	1100	0.49	111	105	0	348	14.5	7.6	0.08	2498	2
104	1149	0.49	112	106	0	360	17.0	7.6	0.09	2689	2
105	801	0.51	91	100	0	357	24.8	5.7	0.13	3054	1
106	801	0.51	95	100	0	339	16.0	6.4	0.09	2568	5
107	801	0.51	100	100	0	316	10.9	6.7	0.07	2243	36
108	801	0.44	101	100	0	321	21.7	5.9	0.22	3728	1
109	801	0.44	104	100	0	311	17.1	6.3	0.14	3449	1
110	801	0.44	111	101	0	302	12.6	6.9	0.11	3195	1
111	801	0.43	116	101	0	290	9.4	7.3	0.08	3214	1
112	801	0.43	120	100	0	287	8.1	7.6	0.08	3294	1
113	801	0.47	92	120	0	338	24.1	5.1	0.17	3475	1
114	801	0.46	95	119	0	324	17.6	5.8	0.12	3142	1
115	801	0.46	101	120	0	315	14.1	6.2	0.10	2714	1
116	801	0.47	105	119	0	305	9.8	6.6	0.08	2483	2
117	801	0.46	110	121	0	292	7.5	6.9	0.07	2593	5
118	801	0.34	114	120	0	258	17.1	5.7	0.50	5019	1
119	801	0.35	114	121	0	265	13.8	6.1	0.24	3847	1
120	800	0.36	115	121	0	269	13.5	6.1	0.18	3644	1
121	801	0.38	115	120	0	274	10.9	6.5	0.16	3387	1
122	800	0.39	114	120	0	276	10.5	6.5	0.12	3361	1
123	800	0.41	116	121	0	280	8.5	6.8	0.10	3004	0
124	801	0.43	115	120	0	283	7.6	6.9	0.07	2902	1
125	800	0.43	100	100	0	312	21.6	5.7	0.20	3806	1
126	800	0.44	100	101	0	314	18.1	6.1	0.17	3821	1
127	800	0.46	100	100	0	317	15.5	6.4	0.12	3317	1
128	800	0.49	100	100	0	319	13.5	6.6	0.09	2955	1
129	800	0.52	99	100	0	311	9.3	6.6	0.06	2213	45
130	1004	0.34	153	115	0	264	7.0	8.7	0.14	3266	1
131	1004	0.34	157	127	0	264	5.4	8.9	0.12	3117	1
132	1003	0.29	145	123	0	242	12.7	7.0	0.36	3024	1

	Engine operating conditions								Engine emissions		
Data point	N (r/min)	Φ	P_m (kPa)	T_m (°C)	EGR (%)	T_{exh} (°C)	CA50 (deg CA)	IMEP (bar)	CO (%)	HC (ppm)	NO_x (ppm)
133	1004	0.37	134	119	0	275	9.0	7.7	0.12	3022	1
134	1003	0.34	133	117	0	270	12.6	7.1	0.19	2992	1
135	1003	0.37	126	128	0	287	10.5	7.1	0.14	2945	1
136	1003	0.36	125	133	0	284	11.0	6.9	0.15	2932	1
137	1003	0.39	118	132	0	297	11.9	6.7	0.13	2602	1
138	1003	0.42	117	129	0	303	9.9	7.0	0.09	2512	1
139	1003	0.43	109	124	0	323	14.7	6.5	0.11	2389	1
140	1003	0.46	108	120	0	329	13.4	6.8	0.09	2329	1
141	1003	0.48	104	116	0	341	15.9	6.6	0.09	2164	3
142	1003	0.44	104	116	0	340	23.4	6.0	0.14	2628	1
143	1003	0.52	97	115	0	371	19.6	6.3	0.10	3259	2
144	1003	0.54	97	117	0	359	14.1	6.5	0.07	2071	28
145	1004	0.48	123	65	0	333	14.6	8.9	0.08	3246	3
146	1004	0.45	133	72	0	310	11.2	9.2	0.08	3262	2
147	1004	0.41	133	79	0	296	12.8	8.6	0.12	3297	2
148	1004	0.38	144	94	0	277	9.5	8.9	0.12	3240	1
149	1004	0.31	145	104	0	246	15.8	7.3	0.61	3263	1
150	1003	0.54	100	77	0	381	22.5	7.0	0.09	2770	2
151	1003	0.53	106	72	0	362	17.0	7.6	0.08	2457	9
152	1003	0.52	108	70	0	353	16.5	7.8	0.07	2561	11
153	1003	0.54	102	65	0	384	23.6	7.2	0.08	2454	5
154	1003	0.46	130	64	0	319	10.7	9.1	0.07	3393	4
155	1003	0.52	107	64	0	364	18.9	7.7	0.08	2797	4
156	800	0.40	118	120	0	285	8.4	6.9	0.10	2948	2
157	800	0.40	119	121	0	281	7.9	6.9	0.09	3038	1
158	800	0.40	119	120	0	278	8.2	6.9	0.09	3002	1
159	800	0.40	120	121	0	277	8.4	6.9	0.10	3005	1
160	800	0.40	118	121	0	275	9.1	7.0	0.11	3151	1
161	800	0.40	119	121	0	274	9.7	7.0	0.12	3237	1
162	800	0.40	119	121	0	273	10.5	7.0	0.13	3399	1
163	800	0.40	117	121	0	271	11.8	6.9	0.13	3552	1
164	811	0.71	89	80	0	400	13.4	5.6	0.05	1808	1301
165	811	0.72	89	83	0	393	11.5	5.5	0.05	1762	1320
166	811	0.71	89	86	0	387	10.9	5.4	0.04	1676	1505
167	811	0.72	89	88	0	384	10.1	5.4	0.04	1680	1523
168	811	0.72	89	90	0	382	9.5	5.3	0.04	1618	1654
169	811	0.69	89	91	0	382	10.7	5.3	0.05	1894	1064
170	810	0.69	89	94	0	380	9.9	5.2	0.05	1708	1063
171	810	0.69	89	97	0	377	9.3	5.2	0.05	1664	1099
172	810	0.70	89	99	0	370	8.2	5.1	0.04	1613	1345
173	810	0.69	89	99	0	372	8.8	5.1	0.04	1549	1255
174	810	0.67	89	109	0	378	9.7	5.0	0.07	2309	679
175	810	0.67	89	112	0	369	9.0	4.9	0.05	1716	869
176	810	0.67	89	115	0	371	9.6	4.9	0.05	1710	789
177	810	0.67	89	118	0	367	8.6	4.9	0.05	1735	766
178	810	0.67	89	120	0	365	8.2	4.8	0.05	1678	804
179	810	0.67	89	122	0	362	8.2	4.8	0.05	1649	885
180	810	0.66	89	122	0	359	8.1	4.8	0.05	1606	900
181	810	0.66	90	123	0	365	8.4	4.8	0.05	1706	699
182	910	0.60	90	101	0	361	7.5	4.7	0.04	1634	473
183	810	0.59	99	115	0	368	15.1	5.1	0.09	3213	5
184	810	0.58	101	115	0	359	14.4	5.2	0.09	3090	7
185	810	0.57	104	115	0	349	11.7	5.2	0.09	3477	3
186	810	0.52	111	116	0	326	9.3	5.3	0.09	3740	2
187	810	0.51	114	115	0	318	8.1	5.3	0.10	3874	2
188	810	0.49	116	115	0	311	7.5	5.3	0.10	3920	2
189	810	0.46	120	115	0	305	7.7	5.3	0.11	4048	1
190	809	0.44	123	115	0	298	8.7	5.3	0.13	4255	2
191	809	0.42	127	115	0	286	6.7	5.4	0.13	4100	1
192	809	0.41	130	115	0	282	6.2	5.4	0.14	4139	1
193	810	0.39	135	115	0	271	6.5	5.4	0.14	3950	2
194	810	0.38	138	115	0	264	5.9	5.4	0.15	3941	2
195	811	0.39	131	103	0	264	16.0	4.8	0.35	5127	1
196	810	0.39	132	105	0	275	12.1	5.3	0.28	4950	1
197	810	0.41	132	106	0	278	8.7	5.6	0.17	4400	1
198	810	0.43	132	108	0	283	6.3	5.8	0.11	4063	1
199	810	0.43	132	109	0	285	5.5	5.9	0.10	3925	1
200	810	0.45	132	110	0	286	4.5	5.9	0.07	3083	1
201	810	0.45	132	110	0	287	5.3	6.0	0.08	3752	1
202	810	0.43	124	116	0	291	9.1	5.2	0.16	4279	1
203	860	0.43	125	115	0	296	9.9	5.3	0.15	4122	1

	Engine operating conditions								Engine emissions		
Data point	N (r/min)	Φ	P_m (kPa)	T_m (°C)	EGR (%)	T_{exh} (°C)	CA50 (deg CA)	IMEP (bar)	CO (%)	HC (ppm)	NO_x (ppm)
204	907	0.42	124	116	0	295	11.0	4.7	0.23	4739	1
205	907	0.49	126	114	0	314	6.0	6.0	0.08	3688	1
206	955	0.49	125	114	0	318	6.6	6.0	0.07	3349	1
207	1003	0.50	125	115	0	333	9.6	6.0	0.08	3466	1
208	1052	0.50	125	116	0	339	10.0	6.1	0.09	3433	2
209	1099	0.50	126	115	0	350	11.3	6.2	0.10	3674	1
210	1147	0.42	140	126	0	315	8.5	6.1	0.12	3250	1
211	1194	0.42	141	127	0	320	9.7	6.1	0.13	3220	1
212	1243	0.42	140	131	0	327	10.8	6.1	0.15	3378	1
213	1291	0.42	140	133	0	333	12.5	6.0	0.15	3328	1
214	1339	0.42	140	136	0	340	12.7	6.1	0.15	3290	1
215	810	0.61	96	115	0	375	17.1	5.0	0.09	2995	27
216	909	0.44	113	105	0	327	11.1	5.0	0.11	3415	2
217	909	0.46	114	110	0	326	7.0	5.2	0.09	3272	1
218	909	0.47	114	109	0	323	6.4	5.2	0.06	2704	3
219	909	0.48	114	108	0	320	3.9	5.2	0.06	2787	4
220	909	0.38	123	121	0	295	7.1	4.8	0.13	3497	1
221	909	0.40	123	124	0	296	5.3	4.9	0.10	3267	1
222	909	0.42	123	124	0	301	3.5	5.1	0.08	3120	1
223	909	0.43	123	125	0	301	2.4	5.1	0.06	3091	1
224	909	0.43	123	125	0	300	1.9	5.1	0.06	3005	1
225	1015	0.53	124	106	0	359	13.2	6.9	0.07	2908	40
226	1014	0.51	124	115	0	348	8.4	6.0	0.07	2795	31
227	1014	0.50	124	117	0	357	10.4	5.9	0.08	3089	2
228	1014	0.51	124	125	0	338	7.1	5.8	0.07	2721	37
229	1014	0.50	124	127	0	346	7.5	5.7	0.08	2976	8
230	1014	0.49	124	130	0	353	9.8	5.7	0.09	3355	0
231	1014	0.48	124	133	0	350	10.4	5.6	0.09	3323	0
232	1014	0.46	124	136	0	348	12.1	5.3	0.10	3401	0
233	1014	0.45	124	140	0	343	11.4	5.3	0.13	3888	0
234	1014	0.46	124	144	0	338	9.6	5.3	0.10	3325	0
235	1014	0.42	133	148	0	317	7.0	5.2	0.11	3345	0
236	1014	0.39	135	152	0	305	7.4	5.1	0.12	3221	0
237	1014	0.41	135	144	0	310	6.7	5.3	0.11	3211	0
238	1014	0.42	135	140	0	312	6.4	5.4	0.11	3157	0
239	1014	0.42	135	135	0	316	6.5	5.5	0.10	3067	0
240	1014	0.44	135	129	0	319	6.1	5.7	0.08	2884	0
241	1014	0.46	135	126	0	315	5.0	5.8	0.07	2822	0
242	1014	0.42	134	122	0	320	9.2	5.6	0.12	3276	0
243	1014	0.46	135	120	0	315	4.8	5.9	0.07	2826	0
244	1014	0.44	135	119	0	316	5.2	5.8	0.09	2970	0
245	1014	0.63	134	120	23	358	11.6	6.3	0.10	3387	0
246	1014	0.66	132	119	23	367	10.0	6.5	0.12	4046	0
247	1014	0.61	142	123	23	335	6.5	6.4	0.10	3182	0
248	1014	0.59	149	133	24	317	3.0	6.4	0.08	2783	0
249	1014	0.62	128	124	19	363	11.1	6.1	0.11	3457	0
250	1014	0.60	135	126	20	344	7.6	6.1	0.10	3278	0
251	1014	0.57	140	129	21	327	6.1	6.1	0.09	2946	0
252	1014	0.63	129	116	20	370	12.6	6.2	0.12	3704	0
253	1014	0.44	161	155	23	277	3.0	5.5	0.16	2961	0
254	1014	0.60	142	117	22	325	6.3	6.5	0.07	2754	2
255	1017	0.54	124	112	8	354	11.0	5.9	0.10	3394	0
256	1017	0.54	124	115	8	352	10.7	5.8	0.08	3059	1
257	1017	0.52	128	118	8	333	7.9	5.9	0.08	2884	0
258	1016	0.50	130	123	9	335	8.5	5.8	0.09	3261	0
259	1017	0.51	130	128	9	328	5.5	5.7	0.08	2933	0
260	1016	0.49	129	130	9	330	7.3	5.6	0.10	3157	0
261	1016	0.49	129	132	9	323	6.4	5.5	0.11	3237	0
262	1016	0.46	136	136	9	309	5.1	5.4	0.10	3284	0
263	1016	0.44	137	142	9	302	5.0	5.3	0.11	3139	0
264	1016	0.43	137	144	10	300	6.1	5.1	0.13	3341	0
265	1016	0.41	137	147	10	294	6.7	5.0	0.16	3537	0
266	1016	0.39	137	148	9	290	8.4	4.7	0.20	3764	0
267	1016	0.39	137	149	10	286	10.5	4.5	0.26	4045	0
268	1016	0.38	141	152	10	279	7.5	4.7	0.27	3991	0
269	1015	0.33	157	162	11	247	5.2	4.5	0.42	3680	0
270	804	0.49	132	112	9	294	3.1	5.6	0.11	3829	0
271	804	0.47	132	118	9	290	3.8	5.4	0.09	3538	0
272	804	0.46	132	123	10	287	2.8	5.2	0.12	3875	0
273	804	0.45	133	126	9	284	3.4	5.2	0.11	3678	0
274	803	0.42	133	128	9	280	5.3	4.9	0.13	3668	0

	Engine operating conditions								Engine emissions		
Data point	N (r/min)	Φ	P_m (kPa)	T_m (°C)	EGR (%)	T_{exh} (°C)	CA50 (deg CA)	IMEP (bar)	CO (%)	HC (ppm)	NO_x (ppm)
275	804	0.51	133	130	21	291	6.0	5.1	0.16	4034	0
276	803	0.52	133	132	21	294	5.2	5.2	0.12	3624	0
277	803	0.54	133	133	21	297	3.4	5.3	0.11	3674	0
278	803	0.45	139	138	22	269	6.5	4.7	0.20	3962	0
279	803	0.46	140	144	22	270	4.5	4.9	0.17	3759	0
280	803	0.44	140	145	21	260	6.2	4.6	0.21	4038	0
281	823	0.51	118	75	0	328	9.1	5.9	0.08	3591	6
282	823	0.44	126	83	0	307	9.7	5.7	0.15	4572	0
283	823	0.47	127	87	0	308	6.0	6.0	0.08	3674	0
284	822	0.38	136	98	0	274	8.5	5.3	0.27	4744	0
285	823	0.53	109	96	0	336	9.3	5.4	0.09	3329	13
286	803	0.57	104	80	0	366	14.4	5.5	0.10	3666	11
287	803	0.54	104	92	0	357	15.2	5.2	0.09	3262	13
288	803	0.52	112	92	0	333	9.8	5.4	0.09	3397	11
289	803	0.50	118	94	0	319	5.8	5.6	0.09	3886	0
290	803	0.47	127	99	0	302	3.8	5.7	0.09	3698	0
291	803	0.41	133	108	0	279	3.9	5.3	0.13	3982	0
292	803	0.39	134	113	0	273	4.2	5.2	0.15	4068	0
293	803	0.36	135	130	0	262	5.0	4.7	0.18	3945	0
294	803	0.39	129	132	0	272	5.0	4.7	0.14	3749	0
295	803	0.41	123	134	0	287	5.1	4.7	0.12	3739	0
296	803	0.43	115	129	0	301	7.5	4.6	0.12	3720	0
297	803	0.71	115	124	23	330	9.6	5.3	0.07	3087	84
298	803	0.83	115	121	30	353	6.1	5.6	0.08	3495	160
299	802	0.73	118	121	26	322	2.8	5.2	0.07	3125	112
300	802	0.65	123	130	24	329	5.0	5.5	0.09	3676	1
301	803	0.61	129	133	25	314	5.3	5.5	0.11	3686	0
302	802	0.61	130	137	27	311	6.2	5.4	0.11	3653	0
303	802	0.60	133	142	27	304	4.6	5.3	0.12	3808	0
304	802	0.58	137	147	29	294	4.1	5.3	0.12	3524	0